Załącznik 2

1. Kopia artykułu: **Judt W.**, Bartoszewicz J., Analysis of fluid flow and heat transfer phenomenon in a modular heat exchanger, Heat Transfer Engineering, vol. 42, is. 3-4, 2021 (online 2019), wraz z oświadczeniem autorów.
2. Kopia artykułu: **Judt W.**, Ciupek B., Urbaniak R., Numerical study of a heat transfer process in a low power heating boiler equipped with afterburning chamber, Energy, vol. 196, 2020, wraz z oświadczeniami autorów.
3. Kopia artykułu: **Judt W.**, Numerical and Experimental Analysis of Heat Transfer for Solid Fuels Combustion in Fixed Bed Conditions, Energies, vol. 13, is. 22, pp. 6141:1-18, 2020.

Analysis of Fluid Flow and Heat Transfer Phenomenon in a Modular Heat Exchanger

Wojciech Judt & Jarosław Bartoszewicz

Taylor & Francis
Taylor & Francis Group

Check for updates

Analysis of Fluid Flow and Heat Transfer Phenomenon in a Modular Heat Exchanger

Wojciech Judt and Jarosław Bartoszewicz

Chair of Thermal Engineering, Poznan University of Technology, Poznan, Poland

ABSTRACT

The article presents the construction of modular a shell and tube heat exchanger, which is proposed for food industry. Authors analyzed possibilities of applying this type of heat exchanger to recover waste heat from a heating boiler used in food production companies. Recovered waste heat can be utilized for palm oil heating, which is a common ingredient used in food companies. This construction of heat exchanger allows controlling a heating power of realized process by simple adjusting area of heat transfer by a system of valves, by disconnecting subsequent sections of the heat exchanger from the plant, when heat requirement is decreasing. The research was divided into two parts. First analytical calculations, related to the design of the heat exchanger were realized. Subsequently, the power of heat exchanger obtained during analytical calculations was compared to numerical calculations. The numerical analysis allowed to demonstrate that the flow of exhaust gases through the shell side of the heat exchanger is not homogenous. Prepared numerical calculations showed the non-uniform character of flow through the subsequent modules of the heat exchanger.

Introduction

Food production companies require significant amounts of heat for the production process. A primary problem occurring during the production process is controlling the number of substrates necessary for the production process. One of the main substrates, which is often used in food production is water vapor. This component is usually generated in a heating boiler, which is located in the factory area. The analyzed heating device has to provide a large range of operation to provide the required amount of water vapor, needed in the production process. Therefore, it is necessary to control a heating power of heating boiler, producing this substrate for food production.

The significant parameter of heating boilers work is the temperature of exhaust gases. This value has a big influence on the efficiency of the realized combustion process. Estimation of the possible amount of heating power that is recoverable from exhaust gases and transferred to the cooling medium according to the energy balance is defined in Equation (1) [1].

$$\dot{Q} = \dot{m}_{eg} C_{p,eg} \left(T_{i,eg} - T_{o,eg} \right) = \dot{m}_{po} C_{p,po} \left(T_{i,po} - T_{o,po} \right)$$

(1)

Authors performed the analysis of a heating boiler, of nominal heating power to equal to 4 MW and generating 150 kW of waste heat through exhaust gases. It is possible to utilize this heat by an additional, external heat exchanger, which is popularly named as an economizer. Authors of the paper analyzed possibilities of designing a simple construction of a modular heat exchanger, which allows changing the area of heat transfer inside of heat exchanger. It is realized by a system of valves, which can cut off part of installed sections of economizer plant. It allows modifying the heating power of economizer depending on the demand in a production process. Authors analyzed possibilities of recovering waste heat for a food industrial plant, which is using palm oil in a chips production. Scheme of the heat recovery plant is presented in Figure 1. In this scheme, an additional oil heating boiler is presented, whose main task is the combustion of used cooking oil. In this process, economizer also

---

CONTACT Wojciech Judt ✉ wojciech.judt@put.poznan.pl 🖥 Chair of Thermal Engineering, Poznan University of Technology, Piotrowo 3, 60965 Poznan, Poland
© 2019 Taylor & Francis Group, LLC

Nomenclature

A	area of heat transfer, m^2		λ	thermal conductivity, W·m^{-1}·K^{-1}
c_p	isobaric specific heat capacity, J·kg^{-1}·K^{-1}		η	efficiency, %
d	diameter, m		μ	dynamic viscosity, Pa·s
DDES	detached delayed eddy simulation		ν	kinematic viscosity, m^2·s^{-1}
g	thickness, m		ρ	density, kg·m^{-3}
Gz	Graetz number, dimensionless		τ	time, s
k	overall heat transfer coefficient, W·m^{-2}·K^{-1}		ω	turbulence dissipation rate, J·kg^{-1}·s^{-1}
K	turbulent kinetic energy, J·kg^{-1}			
l	length, m		**Subscripts**	
LES	large eddy simulation		a	average
$\dot{m}$	mass flow rate, kg·s^{-1}		b	boiler
Nu	Nusselt number, dimensionless		c	combusted fuel
NTU	number of transfer units		conv	convection
Pr	Prandtl number, dimensionless		e	economizer
$\dot{Q}$	heat flux, kW		eg	exhaust gases
RANS	Reynolds-averaged Navier-Stokes equations		ex	external
Re	Reynolds number, dimensionless		f	fluid
SST	shear stress transport		i	inlet
t	temperature, °C		in	internal
T	temperature, K		o	outlet
Δt_{log}	log mean temperature difference, °C		p	pipe
W	low calorific value of combusted fuel, kJ·kg^{-1}		po	palm oil
			w	wall
Greek symbols				
α	heat transfer coefficient, W·m^{-2}·K^{-1}			
ε	turbulence dissipation rate, J·kg^{-1}·s^{-1}			

can be used for increasing the efficiency of the combustion process realized in the additional heating device.

Analysis and modeling of flow parameters

The temperature of exhaust gases obtained from heating boilers of discussed thermal power is usually about 260 °C. The minimal temperature of exhaust gases in the installation is conditioned by avoiding corrosion conditions when exhaust gases reach a temperature of water or acids condensation. In situations, where this phenomenon can occur it is necessary to build a shell side of the heat exchanger and a chimney from environmentally resistant materials. The minimal temperature of exhaust gases at the outlet from economizer was assumed as 180 °C to avoid reaching the dew point of water and acids, which can be precipitated from sulfur and nitrogen from the combusted fuel. The temperature of liquefaction of water is described by a dew point dependent on temperature and partial pressure of water vapor in exhaust gases. Liquefaction point of acids from exhaust gases can be obtained according to the expressions presented in paper [2]. In a production process in a food plant temperature of palm oil is about 180 °C [3]. The assumed temperature of palm oil, which are returning from the frying installation is equal to 130 °C.
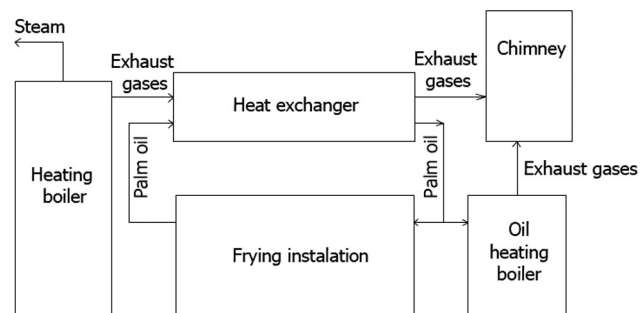

Figure 1. Scheme of a heat recovery plant.

The most common type of heat exchanger applied in food industrial plants is plate heat exchanger construction. This type of heat exchanger has a compact structure. The plate heat exchanger is a good solution for heat transfer realized between fluids in the same state of matter. If the heat transfer occurs between fluid and gas, a shell-and-tube heat exchanger is a better solution. Application of shell-and-tube heat exchanger allows for directing a stream of exhaust gases on the shell side, which compensates the lower heat capacity of the gaseous medium [4].

The flow of mediums through heat exchanger was assumed as counter-current. The stream of palm oil is located in the tube side of heat exchanger. The flow of exhaust gases is realized through the shell side, where the cross-section of the heat exchanger is

Table 1. Thermodynamic parameters of a fluid, which are taking part in a heat transfer process.

Parameter	Exhaust gas	Palm oil
t_a [°C]	215	155
c_p [J·kg^{-1}·K^{-1}]	1097	2249
ρ [kg·m^{-3}]	0.636	825.4
λ [W·m^{-1}·K^{-1}]	0.04	0.16
Pr [dimensionless]	0.7	47.7
ν [m^2·s^{-1}]	3.28×10^{-5}	4.18×10^{-6}

Table 2. Results of analytical calculations of a heat transfer process in a designed construction of the heat exchanger.

Parameter	Exhaust gas	Palm oil
Re [dimensionless]	13400	400
Nu [dimensionless]	86.2	81.4
α_{conv} [W·m^{-2}·K^{-1}]	140	700
k [W·m^{-2}·K^{-1}]	96	
$\dot{Q}$ [kW]	140	

larger. The mass flow of exhaust gases results from the combustion process in a heating boiler. The mass flow rate of combusted coal was computed from Equation (2).

$$\dot{m}_c = \frac{\dot{Q}_b}{\eta_b \cdot W_c} \qquad (2)$$

The efficiency of the heating boiler was defined as the ratio of the enthalpy growth of the working medium to the chemical energy supplied with the combusted fuel. The efficiency of heating boiler work was assumed as 80%. For analytical calculations, a low calorific value of combusted fuel was assumed as 23 MJ/kg. The mass flow rate of coal, which is necessary for obtaining the required heating power is equal to 0.2 kg/s. The mass flow rate of exhaust gases is taken from the combustion process of solid fuel with combustion air factor equal to 1.8 and is based on the ultimate analysis of combusted coal. The calculated mass flow rate of exhaust gases is equal to 2.15 kg/s and is based on calculations according to the paper [5]. The mass flow rate of palm oil is a result of a requisition of oil amount for a production process and can be variable. For a heat exchanger calculation, authors assumed that average oil demand for a nominal production process and it is equal to 1.3 kg/s.

The process of heat exchanger designing was based on analytical calculations of heat transfer process during heat transfer between exhaust gases and palm oil. Analytical calculations were extended by a numerical analysis, which was composed of steady-state and transient calculations of fluid flow through an economizer.

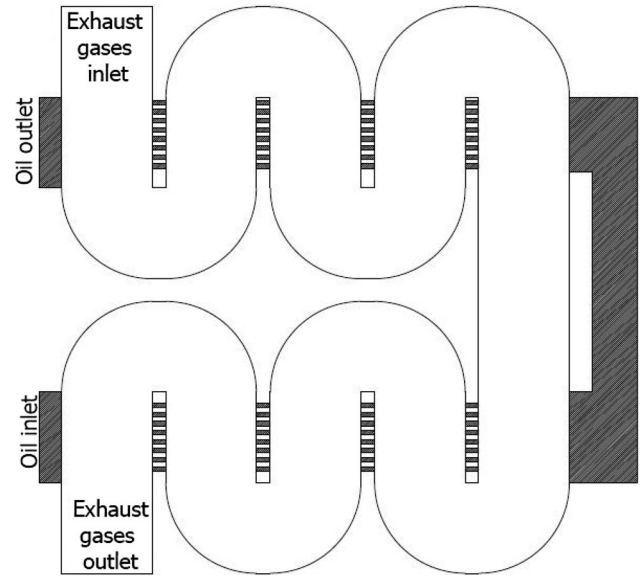## Analytical calculations of the designed heat exchanger

The heat transfer process is realized in a heat exchanger according to Equation (3).

$$\dot{Q}_e = k \cdot A \cdot \Delta t_{log} \qquad (3)$$

Quantity k means an overall heat transfer coefficient, which is described by Equation (4).

Figure 2. Scheme of the analyzed heat exchanger.

$$k = \frac{1}{\frac{d_a}{\alpha_{conv,eg} \cdot d_{in}} + \frac{g_p}{\lambda_p} + \frac{d_a}{\alpha_{conv,po} \cdot d_{ex}}} \qquad (4)$$

The log means temperature difference is described by Equation (5).

$$\Delta t_{log} = \frac{\frac{t_{i,eg} - t_{o,po}}{t_{o,eg} - t_{i,po}}}{ln \frac{t_{i,eg} - t_{o,po}}{t_{o,eg} - t_{i,po}}} \qquad (5)$$

Obtained the log mean temperature difference is equal to 59.4 °C.

Thermodynamic parameters of fluids, which are exchanging heat in a heat exchanger were implemented for an average temperature of each medium. Parameters, which are needed are presented in Table 1 [6,7].

Heat transfer coefficient for exhaust gases was calculated by using a Nusselt number defined by Isachenko in Equation (6) [8]:

$$Nu = 0.26 Re^{0.65} \cdot Pr_f^{0.33} \cdot \left(\frac{Pr_f}{Pr_w} \right)^{0.25} \qquad (6)$$

This expression is used during a flow around the bunch of pipes in the serial configuration. The equation above is appropriate for the Reynolds number

Table 3. Properties for grids used in numerical calculations.

Parameter	The first part of calculations	The second and the third part of calculations
Number of nodes	3.6 million	5.6 million
Number of elements	3.3 million	5.3 million
Maximum orthogonal quality	0.44	0.40
Average orthogonal quality	0.93	0.97
Maximum skewness	0.72	0.70
Average skewness	0.16	0.14

range of 10^3–10^5 and when the Prandtl number range of 0.7–470.

Heat transfer coefficient for palm oil was calculated by using a Nusselt number defined by Sieder and Tate in Equation (7) [9].

$$Nu = 1.86\left(Re\Pr\frac{d}{l}\right)^{0.33} \cdot \left(\frac{\mu_f}{\mu_w}\right)^{0.14} \qquad (7)$$

This equation is defined for laminar flow through a closed duct where Re is less than 2100, Pr range is 0.48–16700, and $\frac{\mu_f}{\mu_w}$ range is 0.0044–9.75, and $(Gz)^{\frac{1}{2}}\left(\frac{\mu_f}{\mu_w}\right)^{0,14} > 2$, where Gz is the Graetz number defined as

$$Gz = \frac{Re\Pr}{l/d} \qquad (8)$$

Results of analytical calculations for both mediums, which are transferring heat are presented in Table 2.

During the analytical calculations, the required area of heat transfer to recover the suitable amount of waste heat is assumed to $24\,m^2$. This value allows estimating the main dimensions of the heat exchanger. Shell-and-tube heat exchanger is built from 64 pipes, which are equally distributed in a heat exchanger geometry. Cross section of shell side of heat exchanger geometry has a square shape with an edge length equal to 0.5 m. Pipes are arranged in subsequent rows, which were not staggered. The diameter of a pipe is equal to 0.019 m. The distance between the axis of the adjacent pipes is equal to 0.06 m. The distance between adjacent pipes is the same in the perpendicular and horizontal side. The heat exchanger is made from a steel plate with a thickness equal to 2.6 mm. Heat exchanger construction for this case is composed of 10 sections, which were arranged into two rows creating two adjacent modules. Each module has 2.5 meters in length. During analytical calculations estimated heating power, for each module is equal to 70 kW, each section of the module can transfer about 14 kW of the heating power.

After each section of the heat exchanger, flow of the palm oil through the pipe side of the heat exchanger can be stopped and the process of heat transfer can be interrupted. It enables to control a heat exchanger power by limiting an area of heat transfer

by leading out a stream of the cooling medium. Area of heat transfer can be changed manually by a worker who will control parameters during the heat exchanger work or by application of automatic system like described in the paper [10]. In situations, where an amount of heating power is higher additional sections of the module can be used in a heat transfer process. Each part of the heat exchanger is connected serially to the next section. Scheme of the designed installation of heat exchanger during analytical calculation is shown in Figure 2. Gray color represents the location of palm oil in the tube side of the heat exchanger. White ducts are representing a flow of exhaust gases through the designed heat exchanger.

Numerical analysis

Numerical calculations were divided into three parts. The first part was based on calculations for the whole geometry of the heat exchanger in a steady state. Calculations in this part were prepared for both modules of heat exchanger separately. Initially, calculations were realized for the first module of heat exchanger construction. After that, results obtained for the first module were implemented to a second model, as a boundary condition. The composition of results from two numerical models shows a whole distribution of fluid flow and heat transfer parameters in the designed geometry. In this part of calculations the Realizable K-ε model of turbulence with enhanced wall treatment application was used. This model is based on the solution of two equations, turbulence kinetic energy equation K and the rate of dissipation of turbulent energy ε. Applied model of turbulence differs from the standard K-ε model by higher ability to capture the mean flow of the complex flow. It is connected with a different formulation for the turbulent viscosity calculation. In addition, higher accuracy of calculations results from the different formulation of the transport equation for the dissipation rate of the turbulent energy. More information about applied models of turbulence can be found in publication [11].

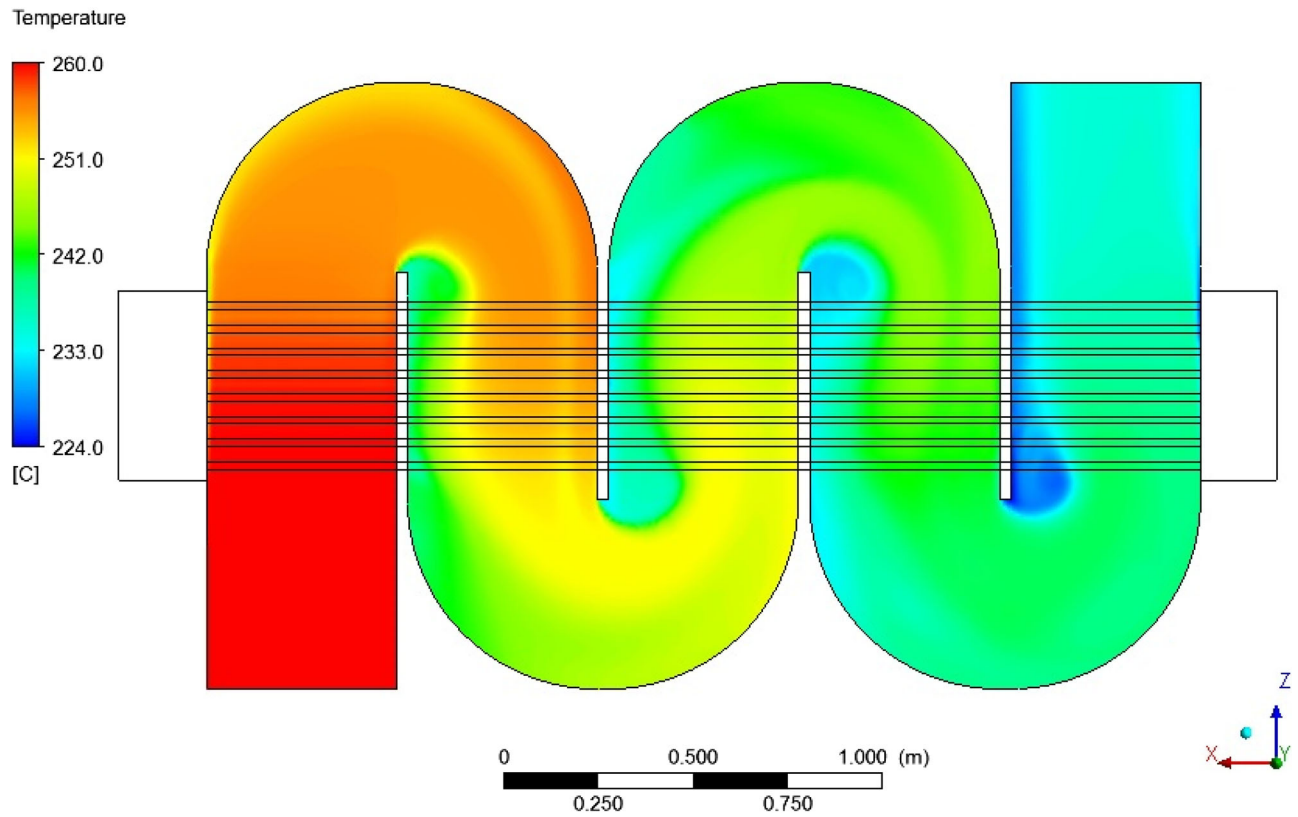The second part of numerical calculations was based on steady-state calculations for two adjacent

Figure 3. The temperature distribution of exhaust gases for a first module of the heat exchanger.
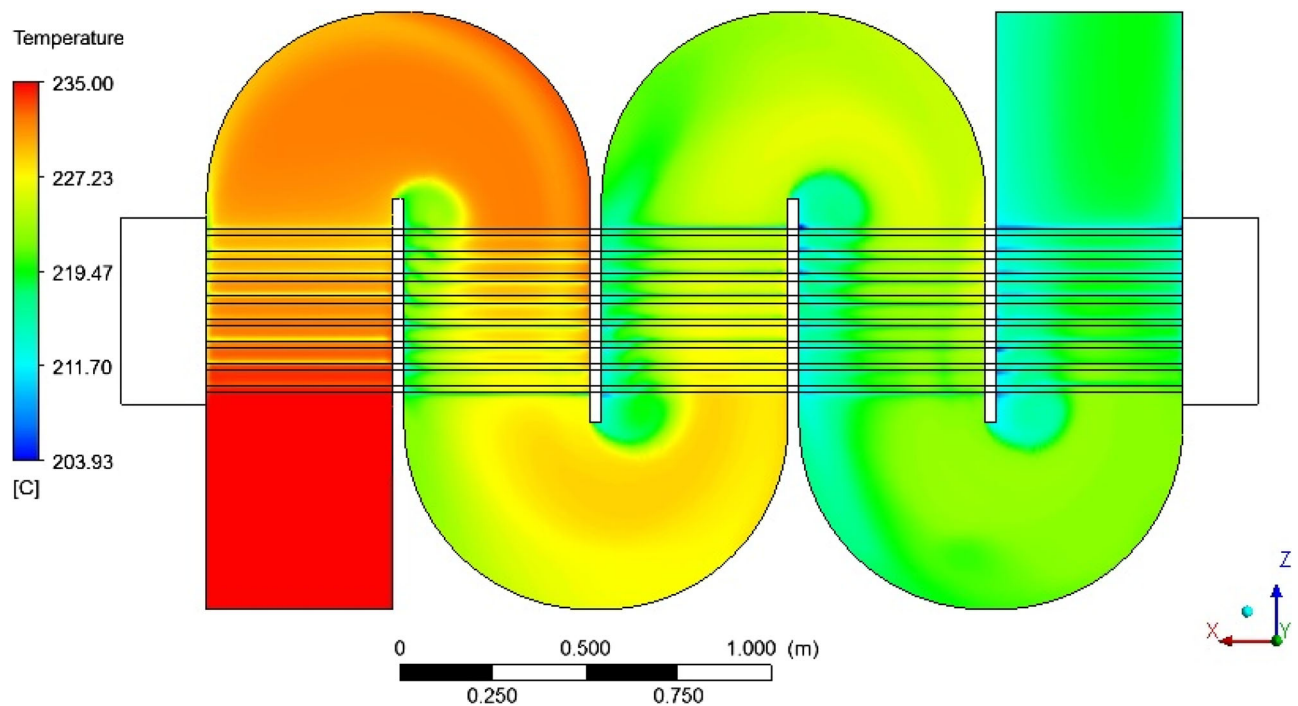

Figure 4. The temperature distribution of exhaust gases in a second module of the heat exchanger.

sections of the heat exchanger. Numerical analysis was realized for the third and fourth section of the economizer, counted from the inlet of exhaust gases to the geometry. Two sections of the heating device were analyzed in the detached model because it is a periodical element of the heat exchanger construction. Realizing numerical calculations for periodical part of the heat exchanger models character of a fluid flow
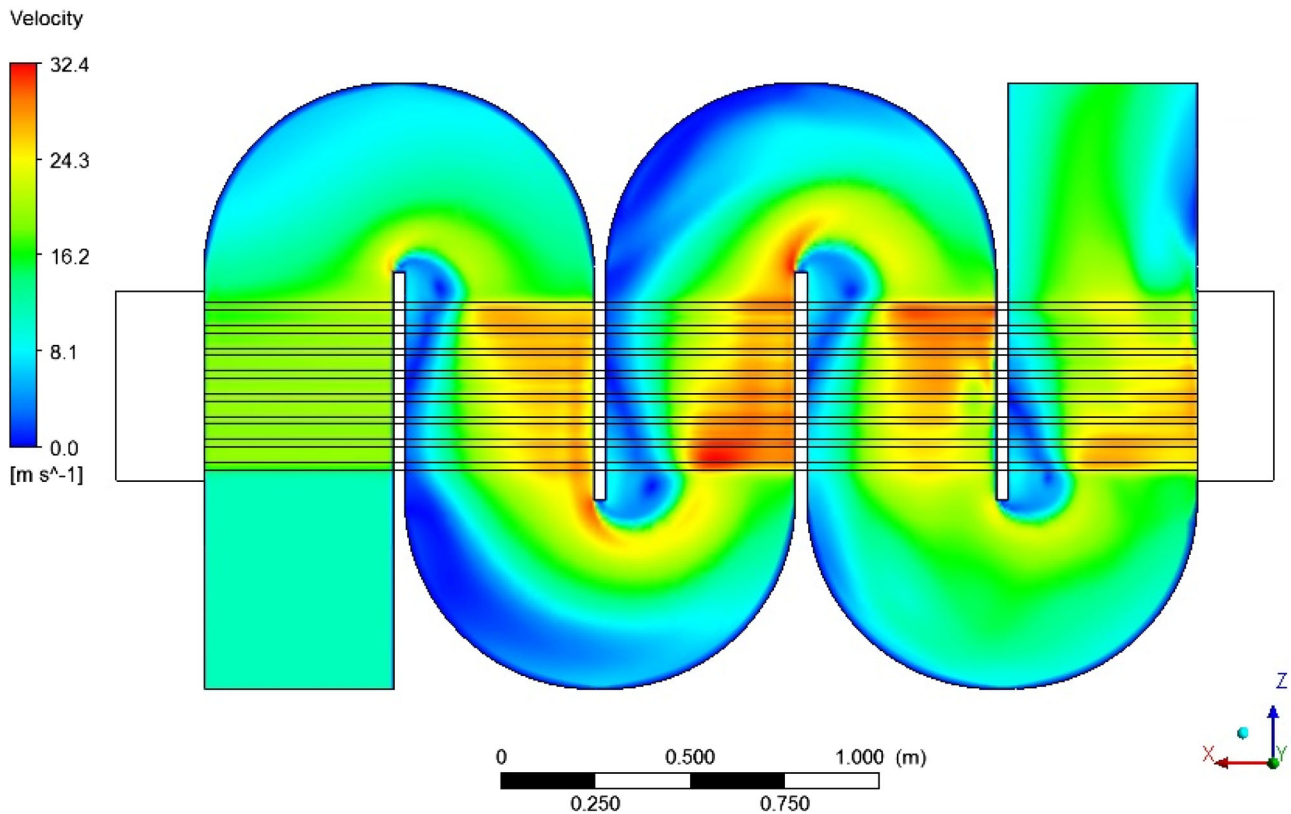
Figure 5. Velocity distribution in a first module of the heat exchanger.

and heat transfer process in this device due to a possibility of using a finer mesh. Boundary conditions for this model originate from a numerical analysis for the first full module of the designed heat exchanger. The boundary condition for the inlet is a temperature and velocity distribution as a profile function obtained in this plane in the first part of calculations. Calculations, which was prepared for a finer mesh, are for using the K-ω SST (Shear Stress Transport) model of turbulence. This model is based on the combination of K-ω and K-ε models. Wilcox's K-ω model is activated for calculation near the wall and the K-ε model is solved in the free stream area. Also, K-ω model is based on the solution of two equations responsible for turbulent kinetic energy K (in the same way as in K-ε) and specific dissipation rate of turbulent energy ω [11].

The third part of numerical calculations was realized also for periodical part of a heat exchanger. The third part of the analysis relied on unsteady calculations of fluid flow in the hybrid modification of the Reynolds-averaged Navier-Stokes equations and Large Eddy Simulation (RANS/LES) models. This type of modeling depends on solving of classical eddy viscosity formulation based on the distance to the wall for cells of fluid adjacent to the

solid boundaries and where a turbulent length scale is less than the grid dimension. Then the calculation is realized by solving the K-ω SST model of turbulence. In the core of a flow where a turbulent length scale exceeds the grid dimension, the solution is based on a sub-grid scale [12,13]. Then a Delayed Detached Eddy Simulation (DDES) model is solved [14]. Initial boundary condition data to this part of numerical modeling was obtained from the RANS calculations in the second part of the numerical investigations.

Information about grids used in numerical calculations is presented in Table 3. The second and third part of calculations were realized on the same mesh. Grids used in numerical calculations have similar skewness and orthogonal quality. DDES mesh is of finer resolution in order to properly resolve exhaust gases eddies.

The accuracy of numerical calculations was realized based on the two main parameters. The first parameter was connected with energy balance obtained between working mediums for every part of realized calculations. Energy difference obtained between working mediums for every part of numerical calculations was less than 0.3%. The second parameter was a comparison of results obtained in a
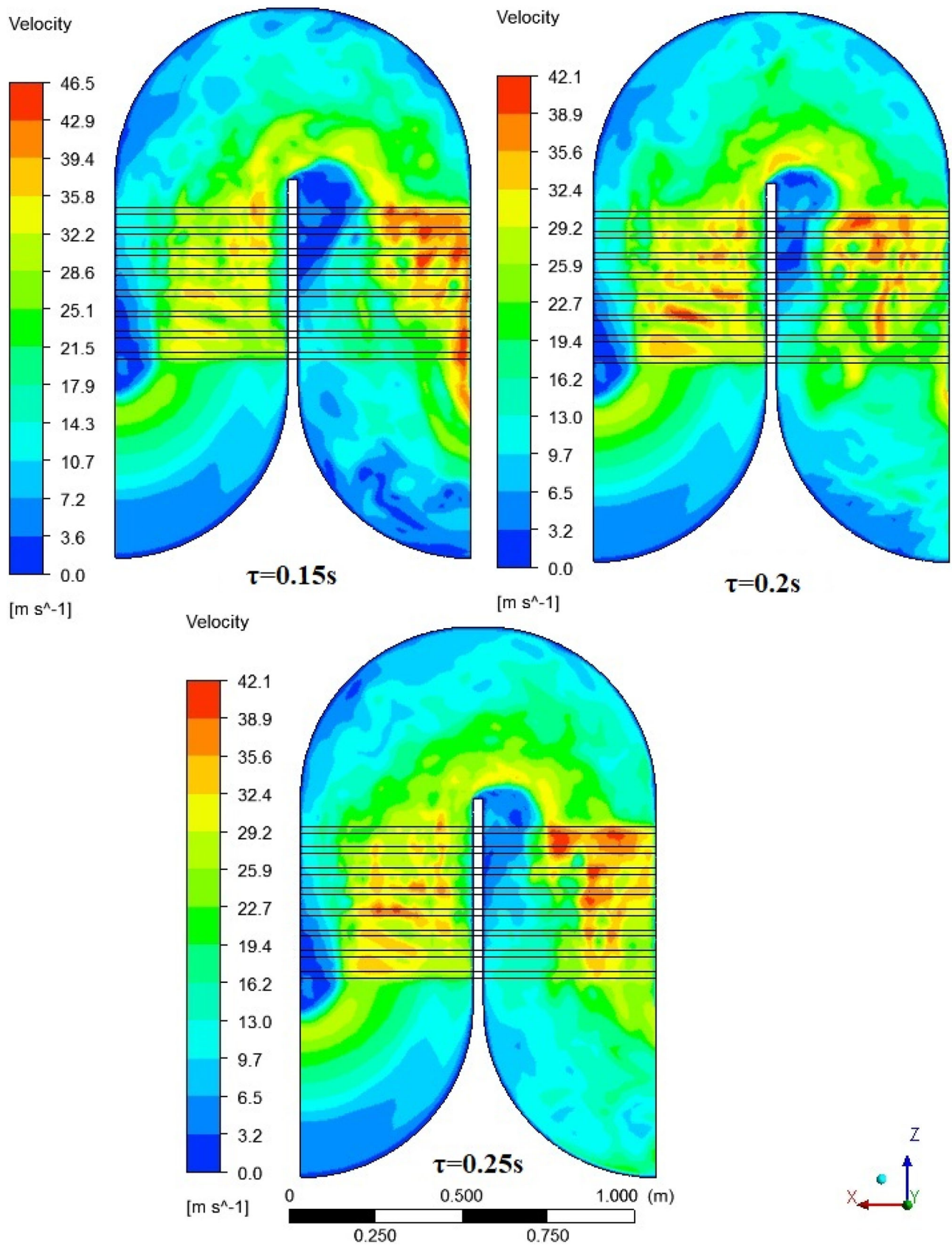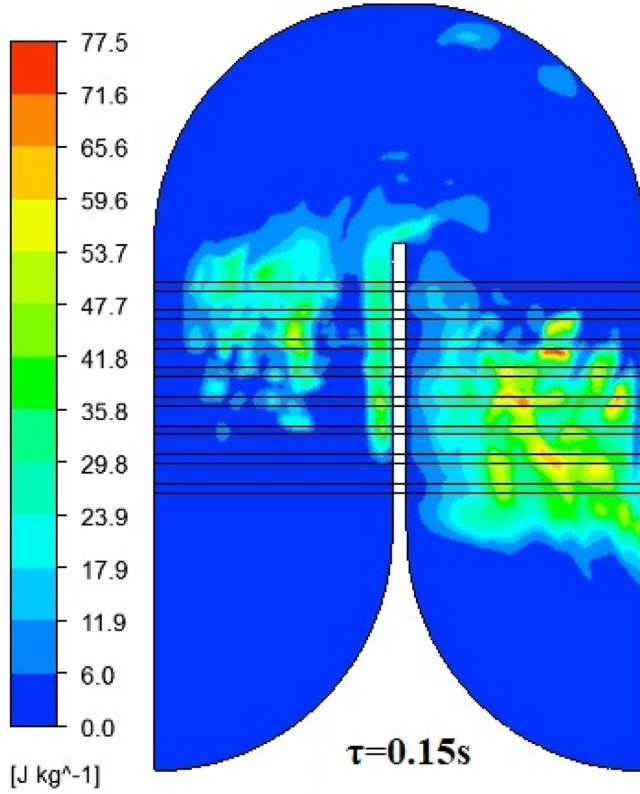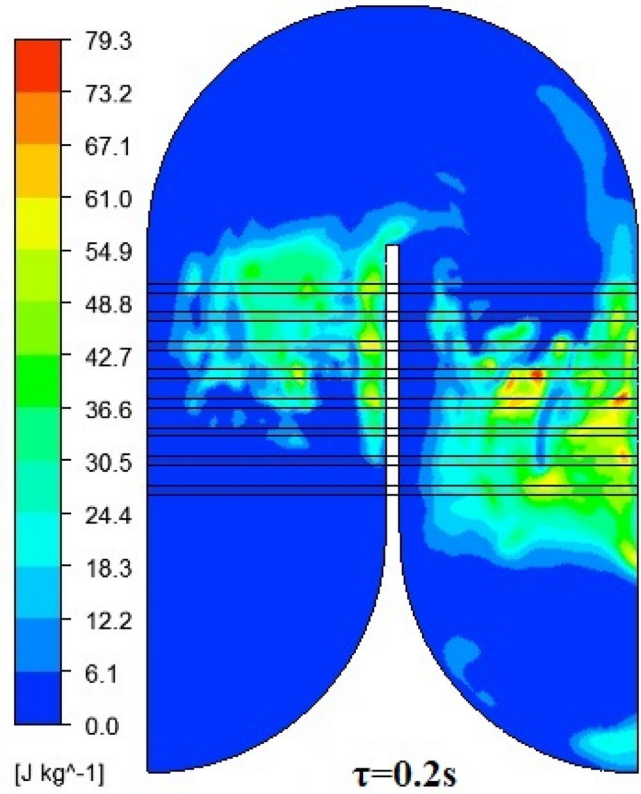
Figure 6. Velocity distribution for one of the sections of heat exchanger obtained for three analyzed time steps.
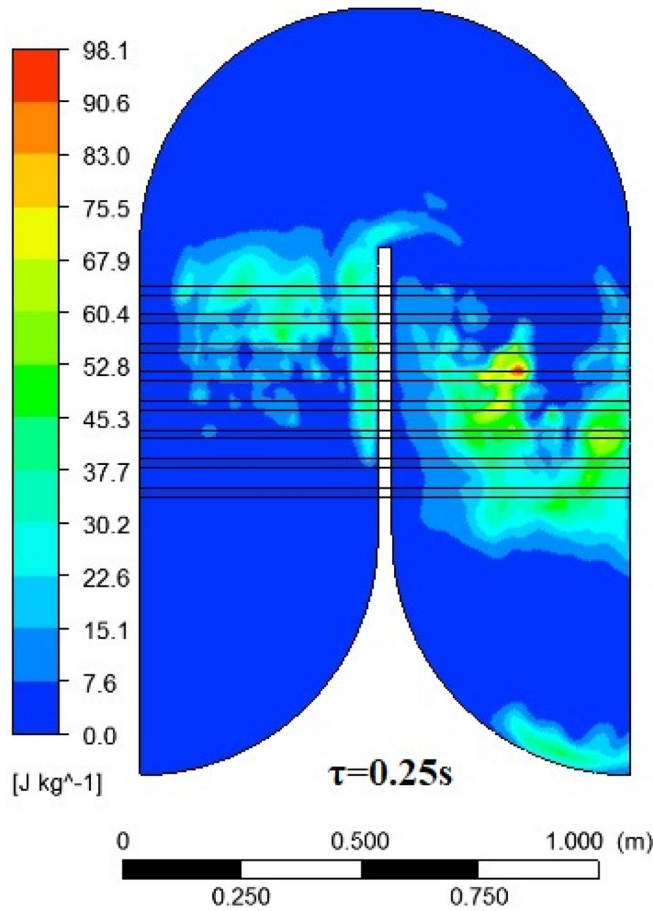
Figure 7. Distribution of turbulent kinetic energy for one of the sections of heat exchanger obtained for three different time steps.

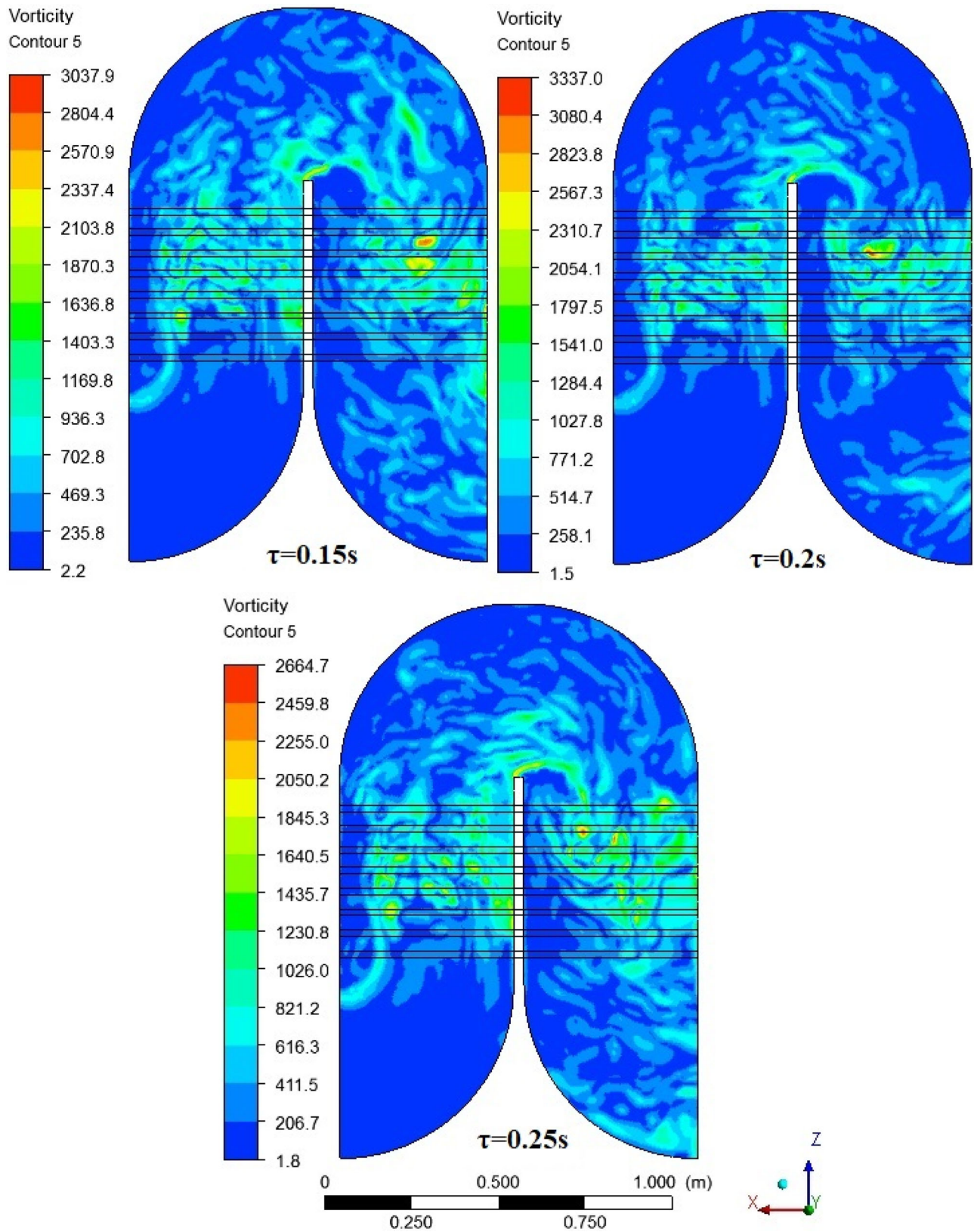**Figure 8.** Distribution of vorticity for one of the sections of heat exchanger obtained for three different time steps.

first and second part of numerical calculations. This comparison shows that the difference in the obtained results for two applied grids was less than 2%.

For each part of the performed analysis, a heat transfer process was realized as an interface between two domains, representing exhaust gas and palm oil

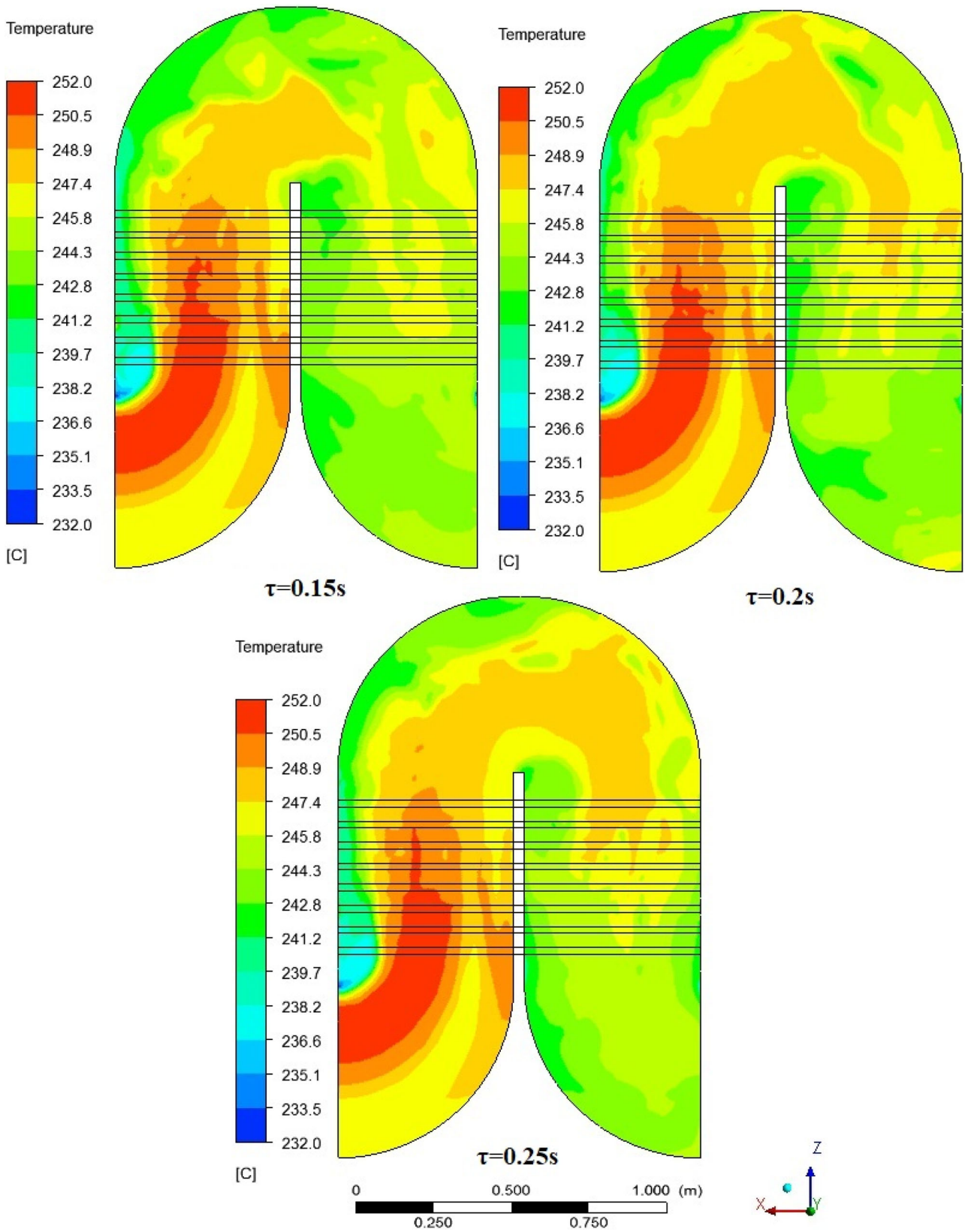**Figure 9.** Temperature distribution for one of the sections of heat exchanger obtained for three analyzed time steps.

location in a heat exchanger volume. Thermal conditions of realized heat transfer are calculated via system coupling. Diaphragm influence for a heat transfer process is implemented to a model in the interface as a steel wall with 2.6 mm thickness. Exterior walls of the heat exchanger are implemented as adiabatic.
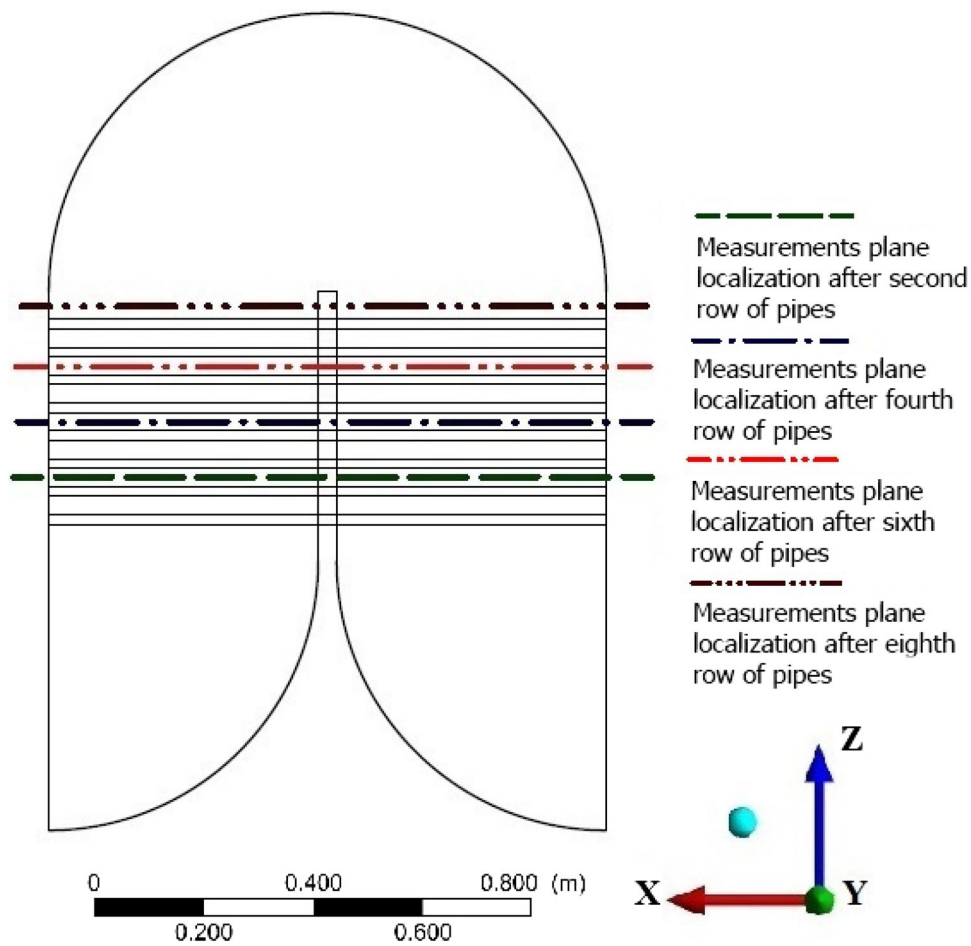
Figure 10. Location of measurement planes for analysis of the character of a fluid realized between the bank of tubes in analyzed sections of heat exchanger construction.

Results

The full construction of the modular heat exchanger

Results obtained for a whole module of designed construction are shown in Figures 3–5. Figure 3 shows a temperature distribution for the first module of the heat exchanger. Distribution of that value for the second module of the designed heat exchanger is shown in Figure 4. Figure 5 presents the whole velocity profile for the first module of the economizer.

Average temperature of exhaust gases at the outlet from the full construction of heat exchanger is equal to 215 °C. It means that a heating power of economizer calculated in numerical modeling is less than the assumption in analytical calculations. A numerical analysis prepared for the full geometry of economizer shows, that the real power of heat exchanger is equal to 106 kW. This value is to 25% less than the heat flow calculated during analytical calculations. This difference results from the inaccuracy of expressions, which were used in analytical calculations of heat

transfer coefficient by convection based on the Nusselt number. However, the reason for power difference is the lack of information about correction factors for the proposed construction of the modular heat exchanger. For a shell-and-tube heat exchanger, the correction factor is depended on the number of baffles located in the construction and the direction of flow [15,16]. Correction factors are connected with pressure drop for a flow of working medium through the heat exchanger, which usually are experimentally defined. Analyzed construction of economizer has a large number of changes in the direction of a flow for which we do not have information about correction factors. The minimal temperature of exhaust gases is equal to 196.7 °C. This temperature is less than an average temperature at the outlet from the heat exchanger but does not achieve a temperature of water or acids liquefaction from exhaust gases. Increasing the power of heat exchanger requires the extension of a heat transfer area by additional modules into the installation. This operation will increase the costs of the construction and will not allow for
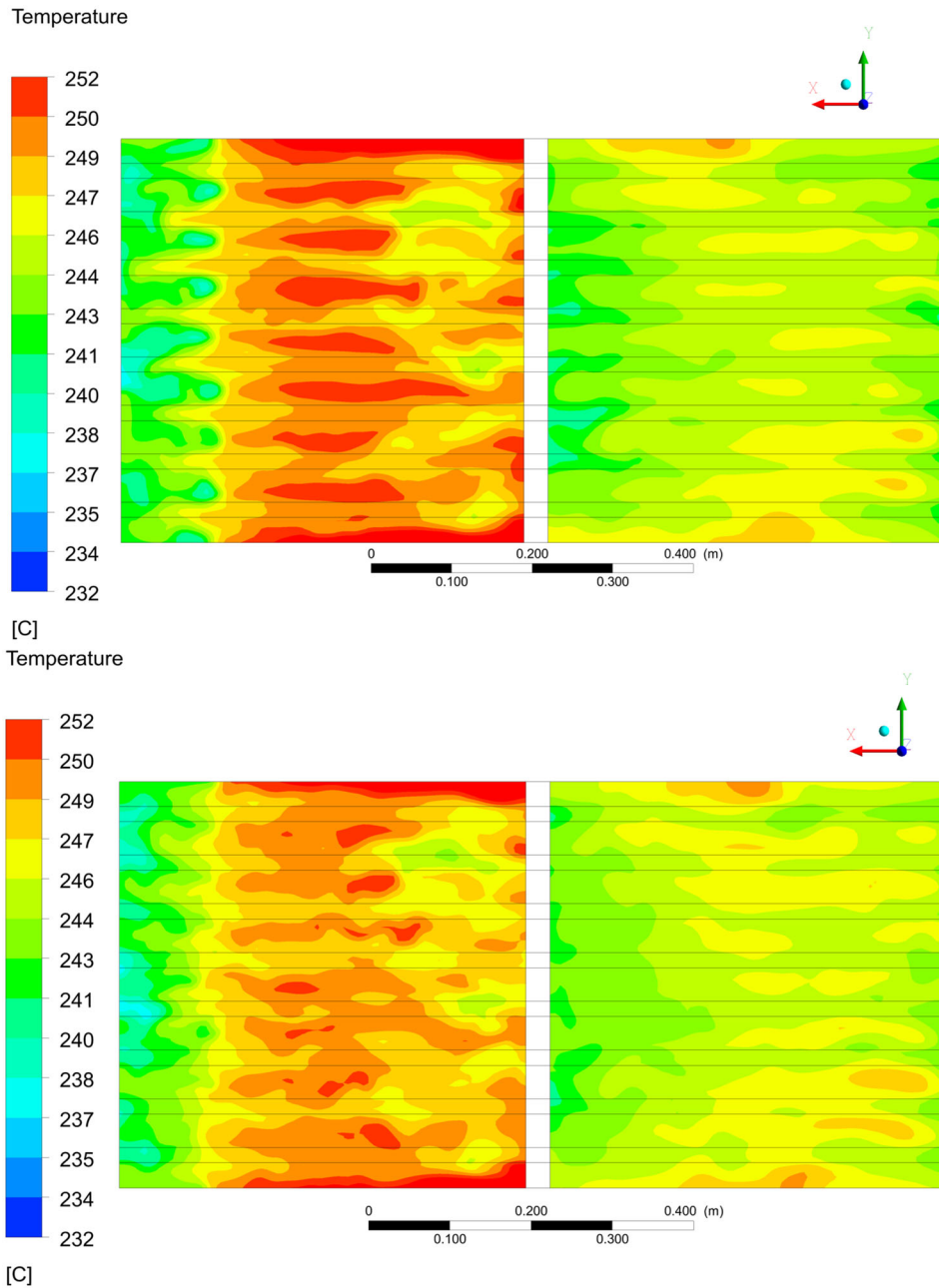
Figure 11. Temperature distribution obtained in the cross-section located after 2 (upper) and 4 rows (lower) of pipes along to the flow in the shell side.

recovering big amounts of waste heat because it decreases the temperature difference between working mediums. Increasing heat transfer area cause the formation of additional area, where heat exchanger walls can be exposed to corrosion conditions.

Analysis of velocity distribution inside designed construction during steady state calculations shows, that fluid flow realized through a heat exchanger has a similar character for each section of the economizer. Exhaust gases changing the direction of flow between adjacent sections of the heat exchanger. It is related to the generation of an eddy in the area

where a change of direction of the flow is present. It is responsible for directing a bigger stream of exhaust gases to the opposite wall of the section. This phenomenon causes that lower amount of exhaust gases are flowing near the wall of the section, which is located closer to the previous section. Owing to this fact also an obtained distribution of temperature in this place is lower because heat transfer from the smaller stream of exhaust gases is easier. Lower velocity of flow causes that the heat exchanger walls located in this place are more exposed to an ash deposition.
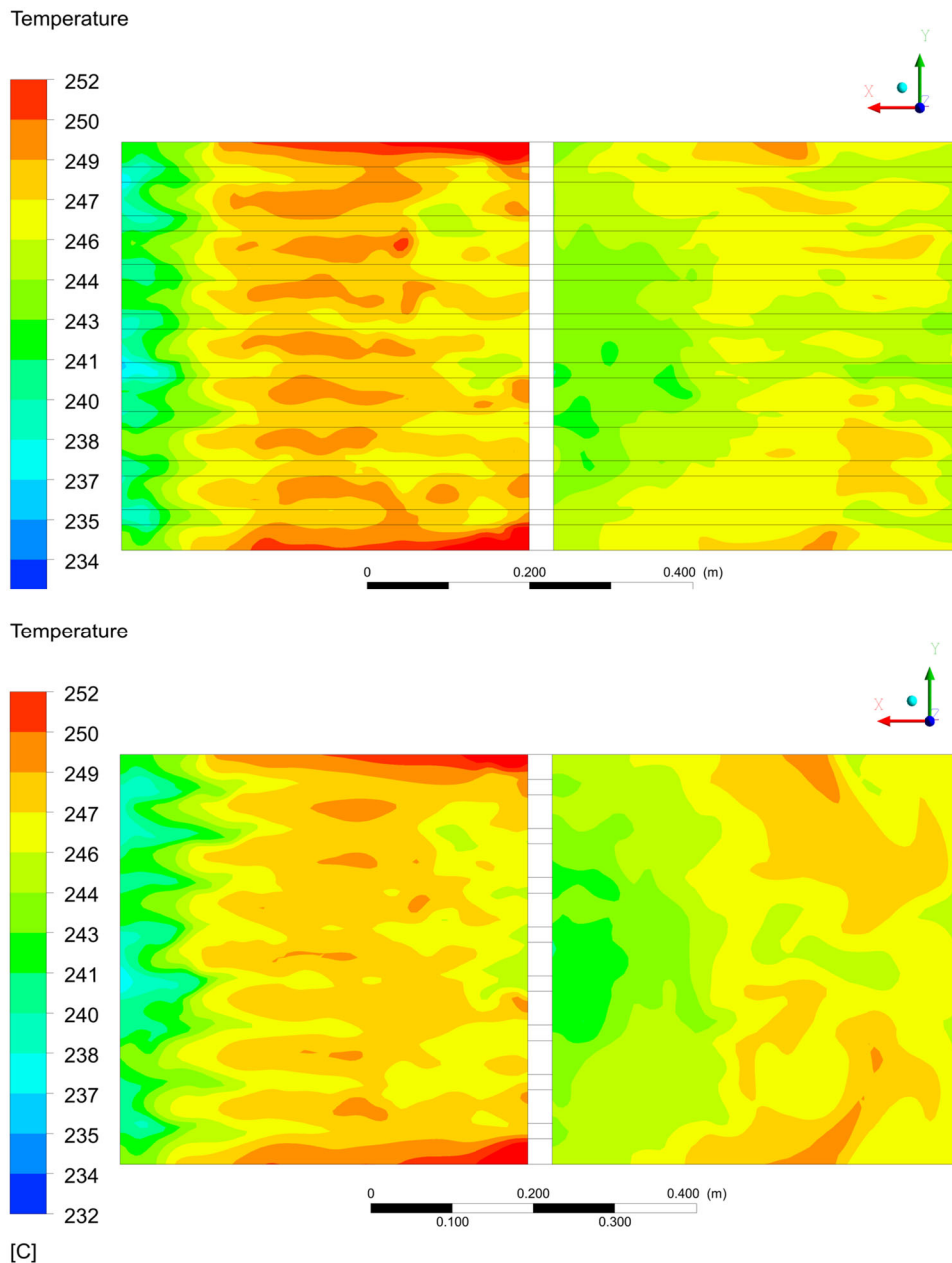
Figure 12. Temperature distribution obtained in the cross-section located after 6 (upper) and 8 rows (lower) of pipes along to the flow in the shell side.

Periodic part of the economizer

Figures 6–9 present parameters of flow and temperature distribution for two adjacent sections of designed construction obtained during transient calculations for a periodical part of the heat exchanger. Results of unsteady calculations are showed as a function of time for three time steps equal 0.15 s, 0.2 s, and 0.25 s. Velocity distribution obtained for that part of the calculation is shown in Figure 6. Obtained results inform that the velocity profile is not homogenous during the heat exchanger operation. Maximum velocity was occurring in the area of tubes, where a cooling medium was flowing. It is related to decreasing cross-section of the shell side of the economizer in this place. Also, a maximum velocity of flow was noticed in different places for further time steps of realized flow. The obtained maximum value of velocity was changing slightly, but noticeably during flow through economizer in considered time steps.

This phenomenon is connected with the variable distribution of kinetic turbulent energy and vorticity in the analyzed flow. Values of those psychical quantities are shown in Figures 7 and 8. Turbulent kinetic energy in numerical calculations for technical application is defined in the same way as in paper [17] and
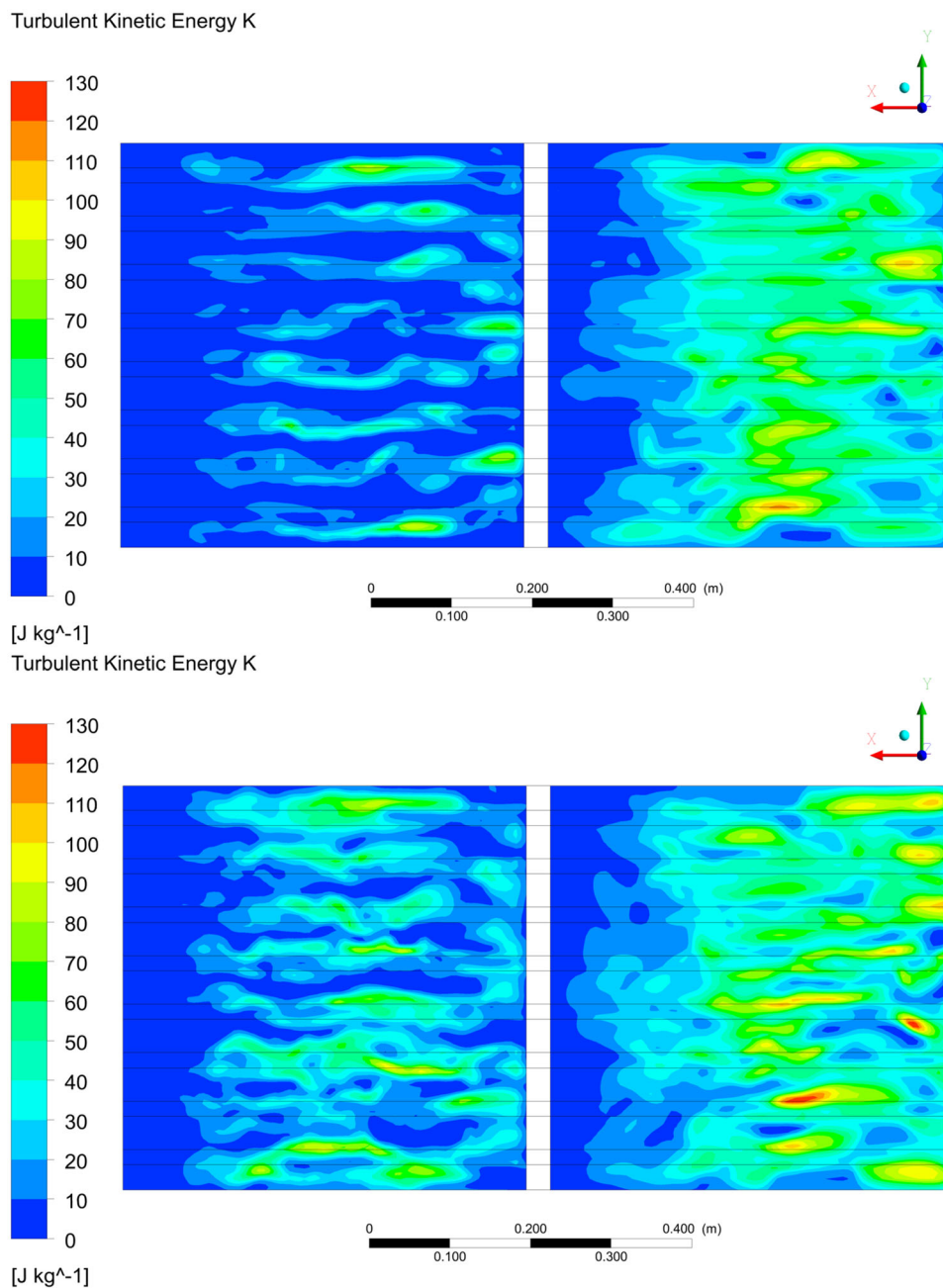
Turbulent Kinetic Energy K

Turbulent Kinetic Energy K

Figure 13. Distribution of turbulent kinetic energy obtained in the cross-section located after 2 (upper) and 4 rows (lower) of pipes along to the flow in the shell side.

describes the intensity of eddies generation inside of flow-through devices. This phenomenon is responsible for the turbulent flow generation between the bank of tubes. During subsequently analyzed time steps the turbulent kinetic energy is changing his distribution. Areas of maximum turbulent kinetic energy are mostly present between pipes in the same row or near to this area. This phenomenon is occurring more intensely on the right side of each section. It is connected with obtained velocity profile for exhaust gases flow through economizer. The higher velocity of the flow is responsible for more intense eddies

generation in this area. Effect of that is visible in the distribution of vorticity. It shows that the peak of vertical flow is occurring in parts of fluid, which are located near to the bunch of tubes. Also, an intense rotational flow is present during changing a direction of flow for exhaust gas between two sections of the heat exchanger. This place is exposed to intense eddies generation, where comes to stagnation of a flow. Eddy generated in this place is responsible for limitation of exhaust gases flowing near to the left side of each section of the heat exchanger, closer to the inlet of the section.
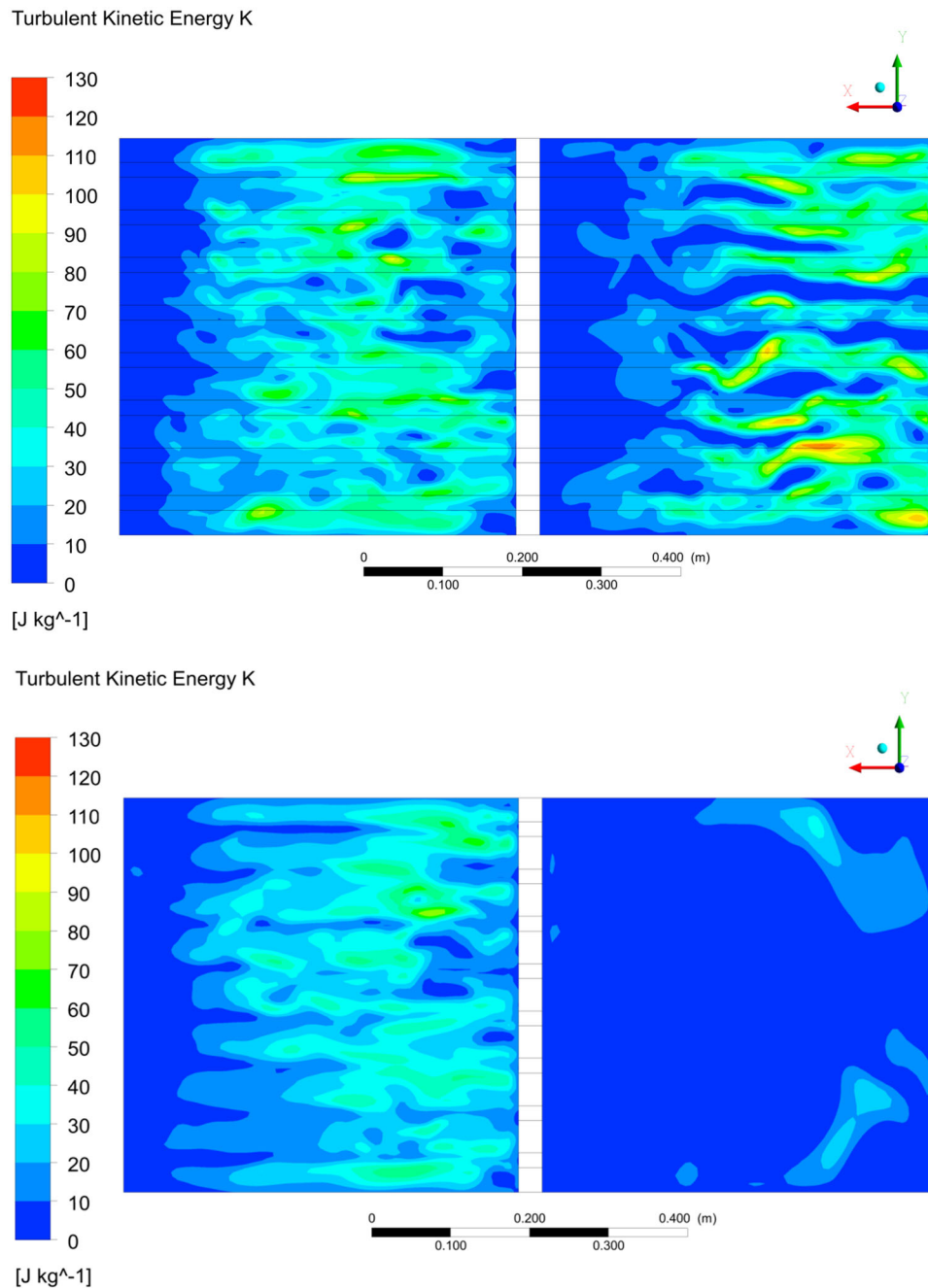
Figure 14. Distribution of turbulent kinetic energy obtained in the cross-section located after 6 (upper) and 8 rows (lower) of pipes along to the flow in the shell side.

Temperature distribution obtained during unsteady calculations is presented in Figure 9. Distribution of temperature was identical for all of the analyzed time steps before changing the direction of flow between subsequent sections of the economizer. When exhaust gases changed the direction, the profile of temperature was changed slightly. The temperature at the outlet from the third section of the heat exchanger for considered time steps was stable and equals to 244 °C. The temperature difference between the inlet to the second section and outlet from the third section was

about 7 °C. Obtained heating power for the analyzed periodical element of heat exchanger construction is equal to 20 kW.

Fluid flow in the area of the bundle of tubes

Authors of paper analyzed the character of flow in designed construction between applied deployment of a bunch of pipes. This part of heat exchanger has a crucial influence on the fluid flow in the whole volume of the heating device. Data were collected for
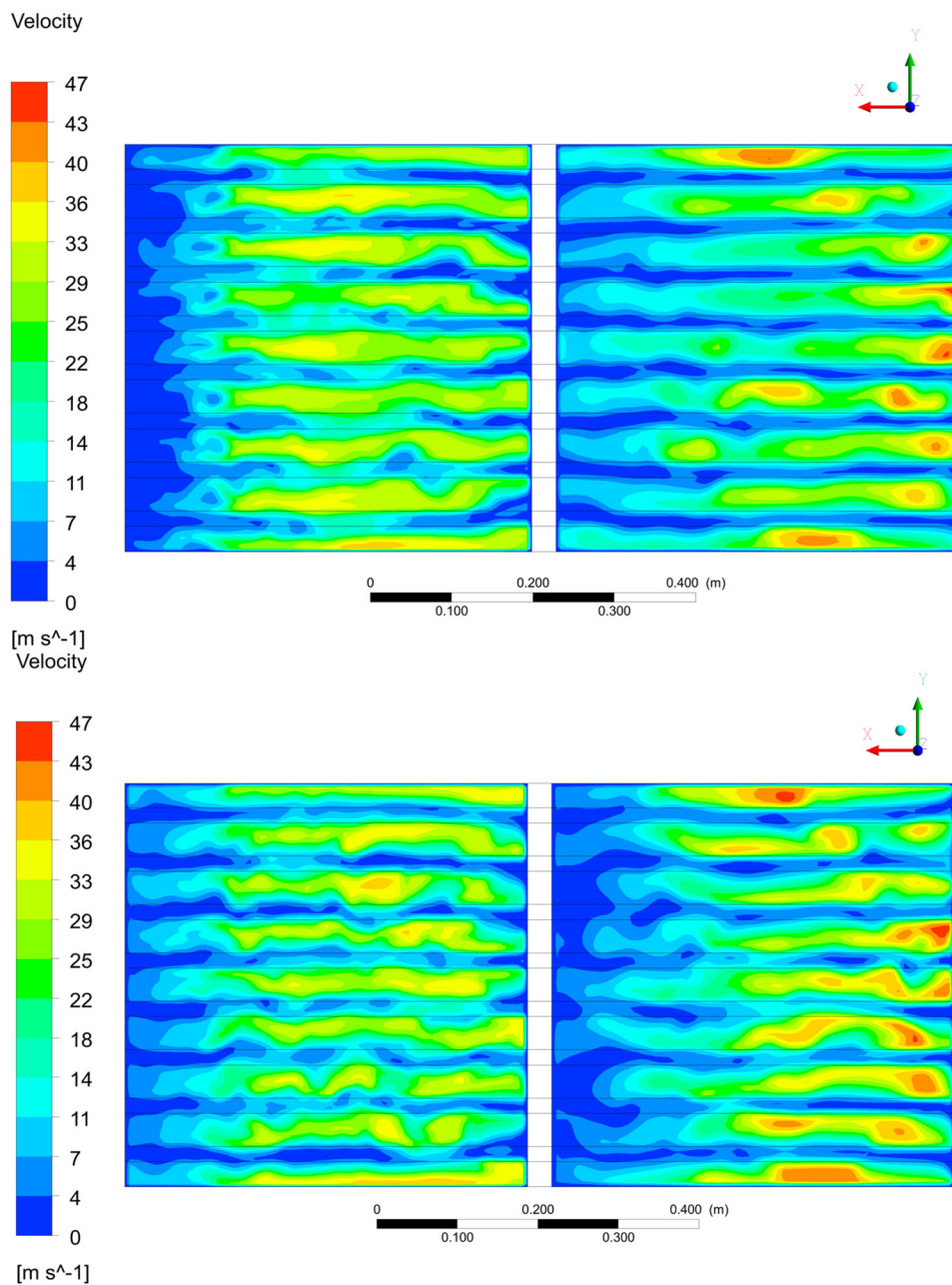
Figure 15. Velocity distribution obtained in the cross-section located after 2 (upper) and 4 rows (lower) of pipes along to the flow in the shell side.

every two rows of pipes, starting after the second row and ending after the eight rows of pipes according to Figure 10. Results are presented in Figures 11–16. Obtained results are presented in the view from above, where the left side of the picture shows a distribution for a previous section of the heat exchanger. The right side of the figure presents data obtained in a subsequent section of economizer located in the same plane. The different direction of exhaust gases flow in adjacent sections of the heat exchanger causes, that presented figures do not show results for the same part of the subsequent section. Results showed

on a cross-section located after the second row of pipes for the first analyzed section will presents results obtained for the subsequent section after the sixth row of pipes according to the flow direction.

Figures 11 and 12 present temperature distribution attained between rows of pipes. The temperature of exhaust gases is dropped gradually in the middle part of the heat exchanger. Part of exhaust gases located near external walls does not change a temperature according to the flow through the first analyzed section of the economizer. This phenomenon is well visible in the upper and lower part of the figure. It is
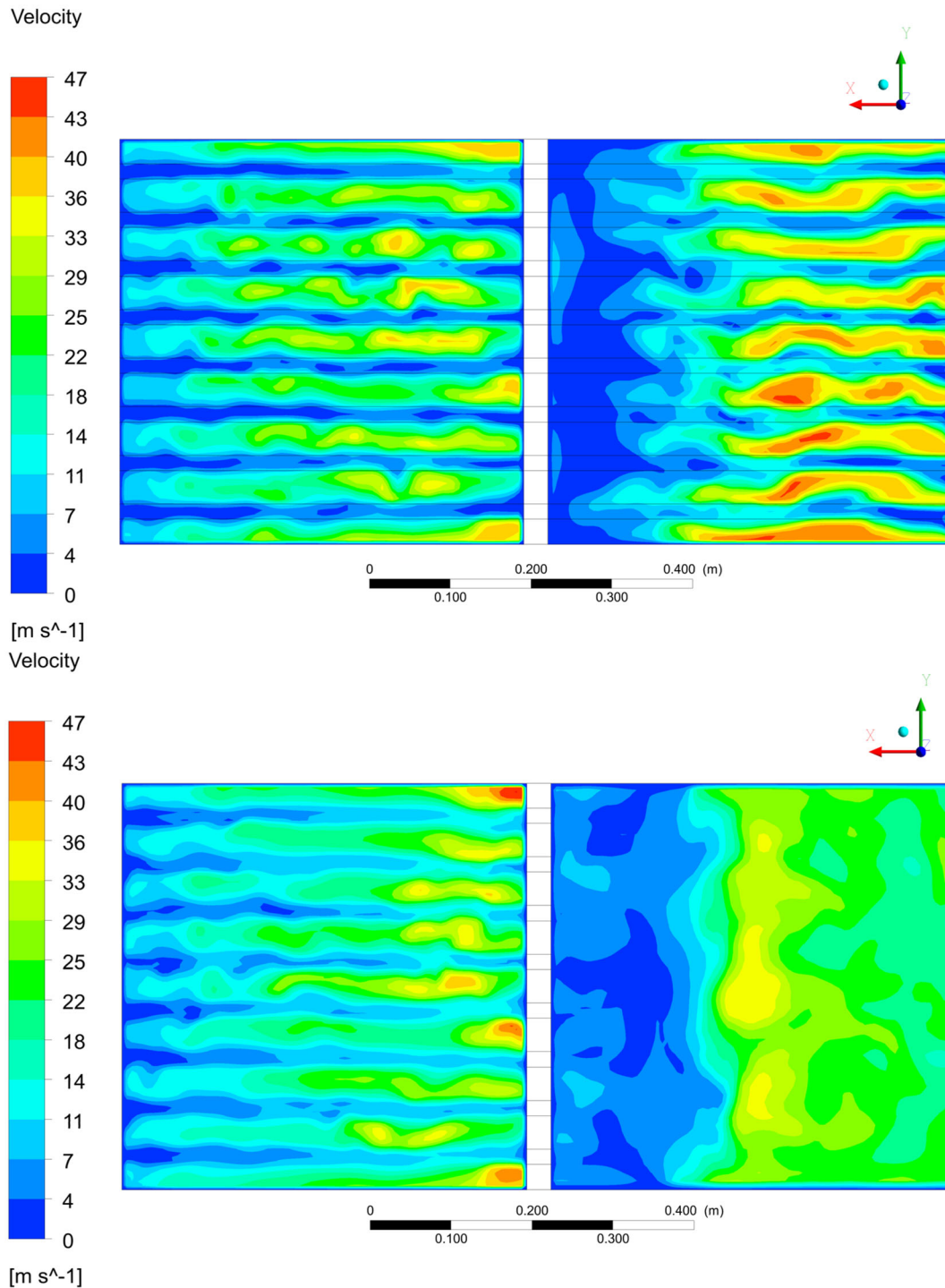
Figure 16. Velocity distribution obtained in the cross-section located after 6 (upper) and 8 rows (lower) of pipes along to the flow in the shell side.

connected with the limited influence of cooling medium for exhaust gas located in this area. In numerical model boundary condition located at external walls of the heat exchanger was assumed as adiabatic.

When exhaust gases are directed into the second analyzed part of heat exchanger most of the flow is directed along the right side of the section. After flow crossing the second row of pipes temperature profile is more uniform. It is connected with a displacement of the exhaust gases stream into the left side of the module and the mixing of exhaust gases. However, a bigger stream of exhaust gases still flows along to the right side of the section. It is visible due to the lower temperature of exhaust gases on the left side of the section.

Velocity distribution and energy of turbulent kinetic energy for a flow, which flows between a bunch

of tubes are presented in Figures 13–16. These parameters have a strong connection with each other so that they can be described together. Obtained results inform that a turbulent intensity is increasing for subsequently analyzed planes for the first modeled section. Delivering of a fluid into the next module with simultaneous changing of a flow direction do not cause limitation of the vorticity parameter for exhaust gases flow. The direction of flow into the next section of a bunch of tubes causes gradually increasing of turbulent intensity of flow. It can denote that flow profile obtained in a previous part of economizer was not fully developed. Transport of the exhaust gases through the second section causes more intense of turbulent kinetic energy generation than obtained in the first section. Flow through second analyzed section did not cause visible increasing of turbulent kinetic energy, which shows that obtained flow in this place is developed. Exhaust gases flow past a bank of tubes causes a big difference in flow distribution between subsequent rows of pipes. Velocity profiles have confirmation in the variable distribution of kinetic turbulent intensity between rows of pipes. In places, where large velocity gradients of flow occurs kinetic turbulent energy has a peak. This area occurs the highest heat fluxes between exhaust gases and oil.

Conclusions

Analysis of fluid flow through heating devices has significant importance for a design process. Numerical modeling allows for a verification of the analytical calculations, which usually form a basis during heat exchanger design process. Appropriate design of a heat exchanger unit enables a long usage of the heating device in a plant. Precise analysis during the design process prevents corrosion [18], which can generate a big amount of costs during maintenance and downtime of installation. Analytical research was connected with mass, momentum, and energy calculations based on the number of similarities for analyzed flow like a Reynolds, Nusselt, and Prandtl number. However, there is a second approach to analytical calculations based on the Number of Transfer Units (NTU) method, which is more precious for the simple construction of heat exchangers. Both methods use correction factors depended on pressure drop and direction of a flow in a shell and tube side of the heat exchanger. However, a lack of information about correction factors causes difficulties in an analytical approach to the calculations of the heat exchanger power. Comparison of these two analytical approaches

will be analyzed in further research. Precious calculation of correction factors required preparation of experimental research for analyzed construction of the heat exchanger. Experimental research and preparation of numerical model also for concurrent flow allows finding diagrams of the heat exchanger efficiency definition, which will be necessary for the application of the NTU method. Numerical calculations showed high asymmetry of a flow in a full construction of the economizer. This phenomenon is presented in the area of reversing chamber responsible for the direction of exhaust gases flow to the subsequent sections of the heat exchanger. Also, it occurs in areas of the shell side of the economizer between the bank of tubes. High asymmetry of a flow distribution means the necessity of preparation numerical calculations for whole sections of the heat exchanger. Approach to the numerical modeling for smaller parts of heat exchanger construction [19,20] causes omission of asymmetry phenomenon in the analyzed flow. Also applied the model of turbulence in the unsteady part of numerical calculations does not allow to obtain accurate results in calculations realized for limited parts of the domain. The occurrence of asymmetric flow through the heat exchanger section is an effect of flow separation. Obtained results during the numerical calculations show area, where is possible to mount flow fences. Application of those elements into the heat exchanger construction will stabilize the character of a flow.

Funding

Notes on contributors

Wojciech Judt is a Ph.D. Student at Chair of Thermal Engineering at Poznan University of Technology, Poland. He received in 2017 a Diploma of M.Sc. Eng. Degree in thermal engineering at the same university. He is currently working on research related to heat transfer process realized in heating boilers for solid fuels and heat exchangers.

Jarosław Bartoszewicz is an associate professor at Chair of Thermal Engineering at Poznan University of Technology, Poland. He received his Ph.D. in 2000 in fluid mechanics. He is currently working on research related to fluid mechanics and heat transfer process in heating devices.

References

[1] S. Fetaka, J. Thibault, and Y. Gupta, "Design of shell-and-tube heat exchangers using multiobjective optimization," *Int. J. Heat Mass Transf.*, vol. 60, pp. 343–354, May 2013. DOI: 10.1016/j.ijheatmasstransfer.2012.12.047.

[2] B. Xiang, M. Zhang, H. Yang, and J. Lu, "Prediction of acid dew point in flue gas of boilers burning fossil fuels," *Energy Fuels*, vol. 30, no. 4, pp. 3365–3373, Mar. 2016. DOI: 10.1021/acs.energyfuels.6b00491.

[3] Y. Chen and G. Moreira, "Modelling of a batch deep-fat frying process for tortilla chips," *Chem. Eng. Res. Des.*, vol. 75, no. 3 part C, pp. 181–190, Sep. 1997. DOI: 10.1205/096030897531531.

[4] I. Afonso, L. Hes, J. Maia, and L. Melo, "Heat transfer and rheology of stirred yogurt during cooling in plate heat exchangers," *J. Food Eng.*, vol. 57, no. 2, pp. 179–187, Apr. 2003. DOI: 10.1016/S0260-8774(02)00296-0.

[5] M. Mittal, C. Sharma, and R. Singh, "Decadal emission estimates of carbon dioxide, sulfur dioxide, and nitric oxides emissions from coal burning in electric power generation plants in India," *Environ. Monit. Assess.*, vol. 186, no. 10, pp. 6857–6866, Jul. 2014. DOI: 10.1007/s10661-014-3894-3.

[6] Pipe Flow Calculations, "Flue gases properties table" [Online]. Available: https://www.pipeflowcalculations.com/tables/flue-gas.xhtml. Accessed: Apr. 4, 2019.

[7] Lipico Technologies, "Technical referencespalm oil properties" [Online]. Available: http://www.lipico.com/technical_references_palm_oil_properties.html. Accessed: Apr. 4, 2019.

[8] V. V. Isachenko, V. A. Osipova, and A. S. Sukomel, *Heat Transfer*, 3rd ed. Moscow: Mir Publishers, 1988.

[9] R. Shankar Subramanian, *Heat Transfer in Flow through Conduits*. Dep. of Chem. and Biomolecular Eng., Clarkson University, [Online]. Available: https://web2.clarkson.edu/projects/subramanian/ch330/notes/Heat%20Transfer%20in%20Flow%20Through%20Conduits.pdf. Accessed: Apr. 4, 2019.

[10] M. Dulău, M. Karoly, and T. Dulău, "Fluid temperature control using heat exchanger," *Procedia Manufacturing*, vol. 22, pp. 498–505, Mar. 2018. DOI: 10.1016/j.promfg.2018.03.058.

[11] H. K. Versteeg and W. Malalasekera, *An Introduction to Computational Fluid Dynamics*, 2nd ed. Harlow: Pearson Education, 2007.

[12] J. Fröchlich and D. Terzi, "Hybrid LES/RANS methods for the simulation of turbulent flows," *Progr. Aerospace Sci.*, vol. 44, no. 5, pp. 349–377, Jul. 2008. DOI: 10.1016/j.paerosci.2008.05.001.

[13] F. Megagnato, B. Pritz, and M. Gabi, "Calculation of the VKI turbine blade LES and DES," *J. Thermal Sci.*, vol. 16, no. 4, pp. 321–327, Nov. 2007. DOI: 10.1007/s11630-007-0321-x.

[14] P. R. Spalart et al., "A new version of detached-eddy simulation, resistant to ambiguous grid densities," *Theor. Comput. Fluid Dyn.*, vol. 20, no. 3, pp. 181–195, Jul. 2006. DOI: 10.1007/s00162-006-0015-0.

[15] P. Stehlik, J. Nemcanský, D. Kral, and L. W. Swanson, "Comparison of correction factors for shell-and-tube heat exchangers with segmental or helical baffles," *Heat Transf. Eng.*, vol. 15, no. 1, pp. 55–65, 1994. DOI: 10.1080/01457639408939818.

[16] B. A. Abdelkader and S. M. Zubair, "The effect of a number of baffles on the performance of shell-and-tube heat exchangers," *Heat Transf. Eng.*, vol. 40, no. 1-2, pp. 39–52, 2019. DOI: 10.1080/01457632.2017.1404806.

[17] R. Stull, *An Introduction to Boundary Layer Meteorology*. Dordrecht: Kluwer Academic Publishers, 2003.

[18] S. Srikanth et al., "Analysis of failures in boiler tubes due to fireside corrosion in a waste heat recovery boiler," *Eng. Fail. Anal.*, vol. 10, no. 1, pp. 59–66, Feb. 2003. DOI: 10.1016/S1350-6307(02)00030-4.

[19] F. Brumercik, D. Sojcak, M. Lukac, A. Nieoczym, and S. Wierzbicki, "Modeling of flow and temperature field in an economizer," *Appl. Comput. Sci.*, vol. 12, no. 2, pp. 63–73, 2016.

[20] M. Almas, "Numerical study of fluid flow over bundle tubes," *J. Electron. Cool. Therm. Control*, vol. 06, no. 03, pp. 109–119, Sep. 2016. DOI: 10.4236/jectc.2016.63010.

Oświadczenie o wkładzie poszczególnych autorów w postanie publikacji naukowej

Wojciech Judt, Jarosław Bartoszewicz, Analysis of fluid flow and heat transfer phenomenon in a modular heat exchanger, Heat Transfer Engineering, 2019, vol. 42, iss. 3-4, DOI: 10.1080/01457632.2019.1699291

Lp.	Imię i nazwisko	Włożony nakład pracy	Udział %	Podpis
1.	Wojciech Judt	Analiza bieżącego stanu wiedzy. Przygotowanie analitycznej analizy wymiany ciepła w wymienniku. Realizacja siatki obliczeniowej oraz obliczeń numerycznych, przygotowanie rysunków oraz tabel. Redakcja tekstu publikacji oraz sformułowanie wniosków.	90%	
2.	Jarosław Bartoszewicz	Zaproponowanie tematu badawczego. Wsparcie merytoryczne.	10%	
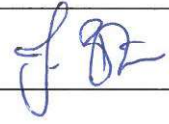
Numerical study of a heat transfer process in a low power heating boiler equipped with afterburning chamber

W. Judt[*], B. Ciupek, R. Urbaniak

Poznań University of Technology, Institute of Thermal Engineering, ul. Piotrowo 3, 60-965, Poznań, Poland

A B S T R A C T

The paper presents a numerical study of a heat transfer process realized in a three draughts low power heating boiler for solid fuels combustion equipped with an afterburning chamber. The main reason for the proposed research is to define the character of an exhaust gas flow through the special construction of heating device at different levels of the heat loading. Heating boiler construction allows for dividing stream of the flue gases into two separated streams. One part of the stream is transferred directly to the afterburning chamber and omits first two draughts of the heating boiler, where the rest of exhausts is directed to. Authors simulated the limitation of exhaust streams division into the afterburning chamber in order optimize the heat transfer process. Obtained results showed that the character of exhaust gas flow strongly depends on the amount of heating power of the heating device. Changes in exhaust gas flow caused increasing of heating power obtained for the nominal load by 4.2%. Similar effect was not visible during heating boiler work with minimal level of the heat load.

© 2020 Elsevier Ltd. All rights reserved.

1. Introduction

Low power heating boilers are very often used in domestic applications as a primary source of heat. Heating systems based on solid fuels are very popular in Polish households. According to Ref. [1] about 35% of energy consumption in the residential sector for heating purposes is related to the hard coal combustion. In The United Kingdom, only 7% of the energy used in single-family houses comes from coal combustion. Effects are well visible in measurements of air quality in the European Union (EU). Poland has the worst air quality among all of the countries of the EU [2]. The main factor responsible for the bad quality of air in Poland is the combustion of low-quality solid fuels and incinerating household garbage by the residential sector. Combustion is often performed in old, uncertified heating boilers, that do not fulfill requirements of efficiency and level of emission of harmful compounds of exhaust gases.

Therefore the European Parliament introduced the Regulation 2015/1189 [3] and 2009/125/EC [4] directive enforcing the implementation of the above. Pack of directives connected with energy savings is popularly named Ecodesign requirements. Article 16 of

the mentioned directive states, that the European Commission is required to implement certain requirements for heating devices, which lead to a limitation of greenhouse gas emission. The requirements cover energy efficiency and air pollutant emissions into the atmosphere. Limitation of pollution is connected with lower fuel consumption by increasing the overall efficiency of heating devices. Mentioned requirements are mandatory from 2020 for all manufacturers and suppliers of solid fuel boilers with a rated heat output of 70 kW or less wishing to sell their products in the EU. According to the directive requirements, heating boilers will be divided into groups according to the seasonal space heating energy efficiency parameter and are labeled just as domestic appliances. Ecodesign defines the parameter of the seasonal space heating energy efficiency according to equation (1).

$$\eta_{son} = 0.85 \cdot \eta_p + 0.15 \cdot \eta_n \tag{1}$$

Parameter η_n is the energy efficiency of the heating device at the nominal heat load. Parameter η_p determines energy efficiency at the minimal power of the heating boiler and depends on the fuel delivery method to the combustion process. Boilers equipped with automatic feeders fall in the range of η_p of 30% of nominal power. Manual feed boilers fall in 50% of nominal power. The above equation is derived from the real heat load of heating boilers used in domestic applications throughout the whole year. The legislator

Nomenclature

A	ash content - wt. %	Δt	temperature difference - °C
c_p	specific heat - $kJ \cdot kg^{-1} \cdot K^{-1}$	η	energy efficiency - %
C	carbon content - wt. %	η_n	energy efficiency at nominal power - %
F	area of cross-section of draught − m^2	η_p	energy efficiency at minimal power - %
H	hydrogen content - wt. %	η_{son}	seasonal space heating energy efficiency - %
$\dot{m}$	mass flow - $kg \cdot s^{-1}$	ρ	density - $kg \cdot m^{-3}$
M	moisture content - wt. %		
N	nitrogen content - wt. %	*Abbreviations*	
O	oxygen content - wt. %	CFD	Computational Fluid Dynamics
p_d	pressure drop − Pa	C1 − C2	line of tubes
P	real power of heating boiler − kW	D_I	first draught
P_n	boiler power level − %	eg	exhaust gas
$\dot{Q}$	heat flux - W	EU	European Union
r	relative flow - %	f	fuel
S	sulfur content - wt. %	max	maximum
t	temperature - °C	out	outlet
u	velocity - $m \cdot s^{-1}$	R1 − R4	row of tubes
W_u	low calorific value of combusted fuel - $MJ \cdot kg^{-1}$	R_x	appointed row of tubes
y^+	dimensionless wall distance	w	water
		z	appointed thermodynamic parameter (density, specific heat, heat conduction, kinematic viscosity)

noticed that 85% of the annual heating boilers work with minimal heating power. The assumed value corresponds with real conditions of solid fuel heating boilers operation during the season.

Improvement of seasonal energy efficiency required to look at a heat transfer process realized in the heating devices. So far the heat transfer process was analyzed usually in high power boilers used in power plants. Source [5] presents a dynamic heat transfer model for the estimation of exhaust temperature for the coal-fired utility boiler. Papers [6−9] raise the issue of a heat transfer process in wall-fired pulverized coal boilers equipped with swirl burners. Heat transfer realized in power boiler superheaters was also analyzed by authors of papers [10−12]. Thermal stresses of critical elements of steam boilers during the heat transfer process were taken into account by Taler et al. [13]. Heat transfer characteristics were also analyzed for large-scale bubbling fluidized bed boilers [14,15], and grate boilers [16,17]. Also, a numerical study is used in the analysis of the heat transfer process in boilers used in thermal plants. Gu et al. [18] analyzed a heat transfer process for supercritical water in riffled tubes with a comparison of heat transfer between smooth and internally ribbed tubes [19] during the steam production. A wide range of information about the limitation of energy waste in industrial boilers is collected in a review proposed by Barma et al. [20].

A Computational Fluid Dynamics analysis prepared for low power heating boilers to a small extent raises the issue of the heat transfer process based on the character of the work of heating devices. A team of researchers from the University of Vigo conducts the numerical simulations of biomass combustion for heat load equal to around 30 kW [21−24]. Numerical calculations were also prepared for the combustion of wood logs in 8 kW stove [25] and wood pellets in a 13 kW heating power stove [26]. The study [27] raises the issue of biomass combustion in small-scale boilers in a simple construction of the combustion chamber. CFD workflow during modeling of fixed-bed biomass combustion in industrial and small scale boilers are presented in Ref. [28]. Coal combustion modeling in small domestic boilers is analyzed in Refs. [29−31]. The application of numerical methods for the definition and optimization of the thermal cycle for low power boilers are shown in papers [32,33]. In an earlier study [34] authors analyzed the temperature

distribution in an outdated type of low power boiler. Paper [35] presents the application of CFD methods for simulation of grate-fired biomass boilers intended for semi-industrial or multi-family residential applications.

However, CFD methods are intensively used for heat transfer and fluid flow analysis in heat exchangers and furnaces intended for industrial purposes. The study [36] deals with heat transfer modeling in modular heat exchanger used as an economizer, which recovers waste heat from a steam boiler. Work [37] raises the issue of conjugate heat transfer in pumped heat energy storage system. Authors of paper [38] analyzed a heat transfer process during cylinder heating in the heat-treating furnace.

Mentioned papers use CFD methods for low power solid fuel boilers do not discuss the inequality of exhaust gas flow through the heat exchanger chamber. Calculations are usually prepared for simple combustion chambers, where the exhaust gas stream is not split into separated parts directed in different directions.

The main objective of the study is the recognition of the character of exhaust gas flow inside the complex construction of a low power heating boiler by CFD methods. Conducted research concerns on the character of the heat transfer process during heating boiler work with various heat load and variable exploitation parameters. The motivation of authors is focused on the improvement of energy efficiency in domestic heating devices based on the real-life operating conditions. In consequence, it leads to the limitation of fuel consumption and, as a result, the reduction of human influence on the natural environment.

2. Setup

The research was prepared for the construction of the heating boiler presented in Fig. 1. The mentioned heater achieves heat load equivalent to 18 kW. Boilers that attain that level of power are designed for domestic applications such as heating and preparation of hot water for sanitary use. The mentioned device is a three draught heating boiler for solid fuel equipped with an afterburning chamber. The location of heating boiler draughts is shown in Fig. 2. Two first draughts are composed of four equidistant pipes arranged in a row. The third draught is composed of eight pipes arranged in
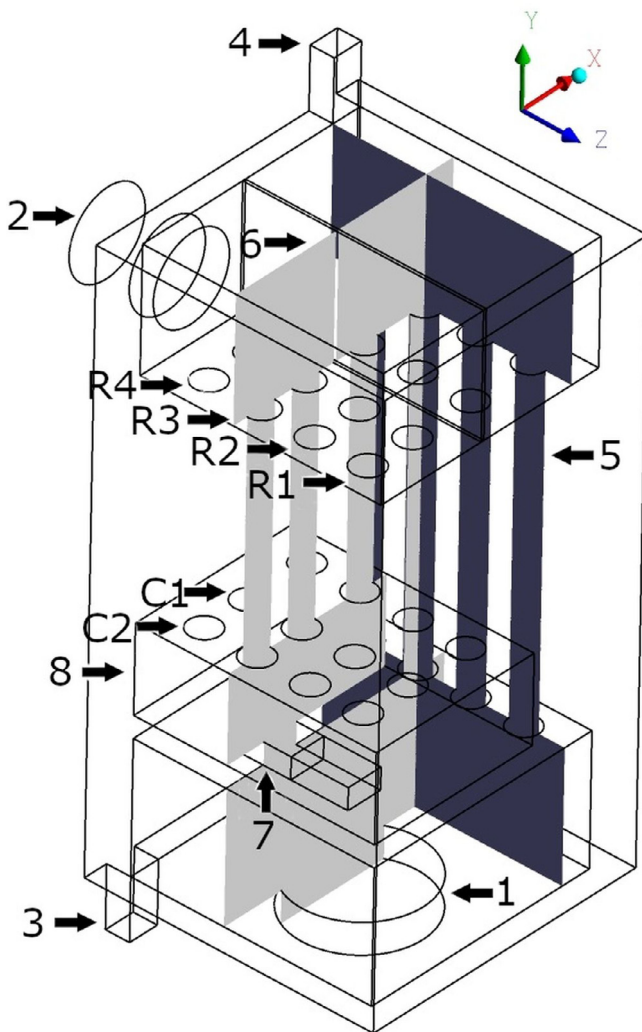
Fig. 1. Construction of the heating boiler with marked crucial planes (XY and YZ) used in results analysis, 1 − combustion chamber, 2 − flue, 3 − water inlet, 4 − water outlet, 5 − plane YZ, 6 − plane XY, 7 − directly connection between combustion chamber and the afterburning chamber, 8 − afterburning chamber, C1-2 − lines of pipes in the draught, R1-R4 - rows of pipes in the draught.

Fig. 2. Draughts location in the heating boiler structure.

two parallel lines. The boiler is designed for coal combustion in the retort burner with automatic fuel delivery.

Construction of the heating device allows for dividing exhaust gases into two separate streams. The operation scheme of the heating boiler is shown in Fig. 3. One portion of the flue gas is directed to the afterburning chamber through the first and second draught. The second portion of fumes flows directly from the combustion area to the afterburning chamber. Two parts of exhaust gas with different temperatures are then mixed inside the afterburning chamber. The main task of that element is to combust flammable compounds present in exhaust gases, which left from the combustion chamber. The third draught is responsible for extracting the fumes from the afterburning chamber into the flue, where gases are disposed into the atmosphere.

3. Methodology

Numerical analysis was prepared for 30% and 100% of the nominal power of the heating boiler. Mentioned levels of the heat load arise from Ecodesign requirements. Calculations were
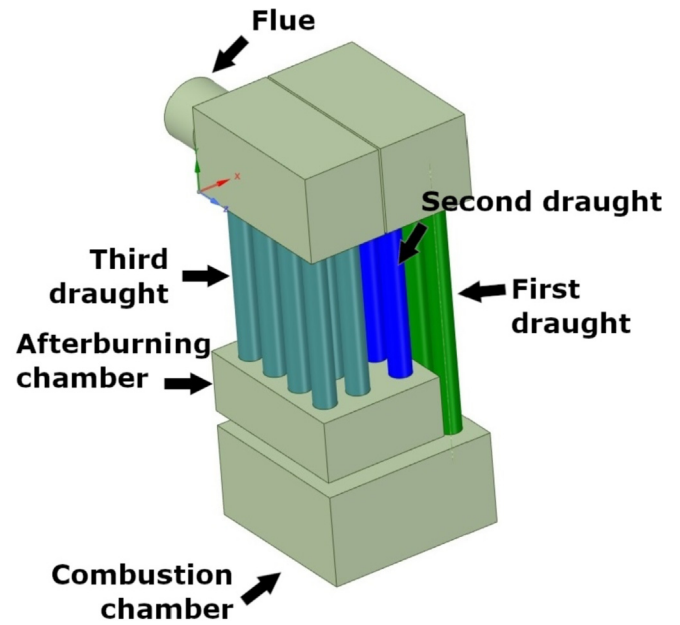
prepared in the ANSYS Fluent environment. The flow is analyzed based on the mass flow rate of exhaust gases, flowing directly to the afterburning chamber. The numerical model predicts two configurations of the duct 7 showed in Fig. 3. In the first case, the flow through the duct is unbound according to the heating boiler construction. In the second case, a cross-section of the duct is limited to 50%. The main reason for that approach is to show, how the heat load will change during the limitation of flow from the combustion chamber to the afterburning chamber and in consequence directing the higher amount of exhaust gas flow through the first and second draught.

3.1. Mesh used in numerical modeling

An unstructured, polyhedral mesh is generated in the Fluent Meshing Software. The quality and sizing parameters of the used grid are shown in Table 1. A boundary layer first element height is prepared for y^+ parameter equal 1. Polyhedral grids combine the advantages of the application of hexahedral and tetrahedral elements. Hexahedral elements are less sensitive for numerical diffusion as tetrahedral grids. Tetrahedral meshes are generated in a convenient way by an application of automatic algorithms that allow for the meshing of complex domains. As a convergence criteria, a balance of energy and mass flow of the working medium is used. Also, a temperature of working mediums at the outlet from the domain was taken as the criterion of the convergence of simulations. Increasing the number of cells in the computational grid does not provide a more accurate solution.

3.2. Boundary conditions

As a working media exhaust gas and water are used. Thermodynamic properties, having an impact on a heat transfer by convection were defined as a function of the temperature of exhaust gas. The parameters are density, specific heat, heat conduction and kinematic viscosity. Values of the aforementioned parameters are derived from properties of primary compounds of the exhaust gas composition as a function of temperature according to the equation (2)
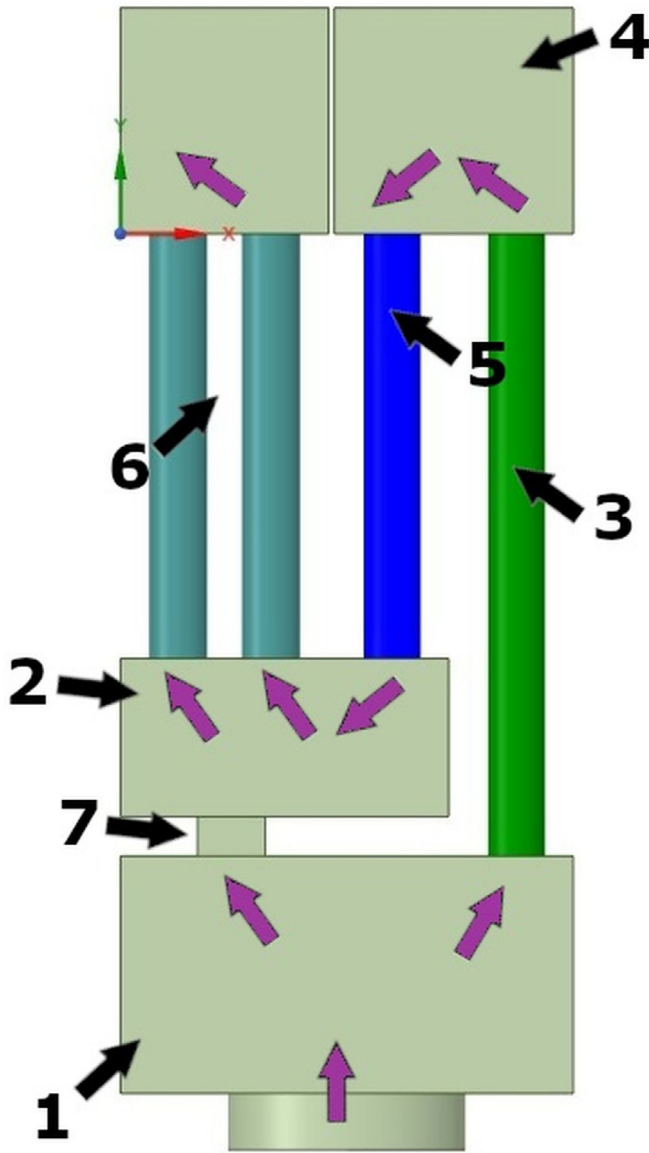
Fig. 3. The operation scheme of heating boiler work, 1 — combustion chamber, 2 — afterburning chamber, 3 — first draught, 4 — reversing chamber, 5 — second draught, 6 — third draught, 7 — channel connecting combustion and afterburning chambers.

Table 1
Parameters of the grid used in the numerical calculations.

Number of elements	Orthogonal quality		Skewness	
	min	ave	max	ave
3.9 mln	0.10	0.83	0.87	0.12

$$z_{t_{eg}} = \sum_{i=1}^{4} P_i \cdot z_{i,t_{eg}} \cdot \frac{273 \text{ K}}{273 \text{ K} + t_{eg}} \qquad (2)$$

where $1 - CO_2$, $2 - N_2$, $3 - O_2$, $4 - H_2O$.

Specific heat, heat conduction and kinematic viscosity for water are defined as a constant and are derived from the average temperature of water in the domain. Usually, a water temperature difference for low power heating boilers ranges between 10 and 15 °C and such temperature difference in this range does not cause a major change in physical properties.

The density of water is modeled as a function of temperature in a range of temperature changes according to Kell's formulation [39]. The omission of the differential density of water as a function of temperature causes problems with the natural mass movements in the water domain. This leads to the adulteration of a local temperature difference between the flue gas and the cooling water and causes flawed computation of heat transfer in the whole domain of the modeled heating device.

Heat transfer by radiation in the modeled heating boiler is simulated by the application of the Discrete Ordinates model of radiation. This method is sufficient for the solution of radiation heat transfer for non-grey problems in semi-finite and finite mediums. The considered model allows for scattering modeling with complete frequency redistribution and continuum absorption [40].

In a numerical model, the k-ω SST (Shear Stress Transport) model of turbulence was used. This model is based on the combination of k-ω and k-ε models. Wilcox's k-ω model is activated for calculation in the inner region of the boundary layer. The k-ε model is solved in the free stream area [41].

Boundary conditions at the inlet to the domain for both fluids are defined as the mass flow. The amount of fuel $\dot{m}_f$ required for obtaining a power of conversion process results from the definition of the efficiency according to the equation (3).

$$\dot{m}_f = \frac{\dot{Q}}{\eta \cdot W_u} \qquad (3)$$

Quantity of exhaust gas $\dot{m}_{eg}$, which is flowing through the domain depends on the power of the combustion process and in consequence from the mass flow of fuel delivered to the burner. The amount of exhaust gas is calculated according to the methodology described in Refs. [42,43]. Calculations are based on the fuel composition according to the equation (4) and originate from proximate and ultimate analysis of the fuel.

$$C + H + S + N + O + M + A = 1 \qquad (4)$$

It is assumed that the proper combustion process of solid fuel occurs at the air exceed coefficient equals 1.8. Mentioned value refers to a practical approach to the research of solid fuel combustion and finds confirmation in other works [44,45]. Basic parameters of coal required in analytical calculations are presented in Table 2. The mentioned composition represents typical hard coal intended for automatic burners in a fraction of grain of 5—25 mm, which is currently available on the Polish market.

The temperature of exhaust gas is specified by the calculation of the real initial temperature of the combustion process [46]. This value is calculated from the calorimetric temperature of combustion with taking into account an excess air number which is equal to 1.8. Analytical calculations were prepared for the nominal power of the device for the composition of exhaust gases calculated before. The temperature at the inlet to the domain is equal to 850 °C. The stream of cooling water, which is flowing through the

Table 2
Composition of fuel used in analytical calculations.

Parameter	Value
Fixed carbon - C (wt. %)	65.6%
Fixed moisture - M (wt. %)	12%
Oxygen - O (wt. %)	9.6%
Ash content - A (wt. %)	8%
Hydrogen — H (wt. %)	4%
Nitrogen - N (wt. %)	0.8%
Sulfur - S (wt. %)	0%

water jacket depends on the power of the heating boiler. Mass flow of water required to receive the desired heating power is defined according to the equation (5).

$$\dot{m}_w = \frac{\dot{Q}}{c_p \cdot \Delta t} \tag{5}$$

The temperature of water at the inlet to the domain depends on the load and size of the installation receiving a generated heat. This value, in this case, is assumed as 60 °C.

Mass flow of exhaust gas and water through the heat exchanging chamber in the analyzed construction of the heating boiler is showed in Table 3. Nominal heating power $\dot{Q}$ is defined for a construction equipped with vortex generators, which are mounted in every tube forming the heating boiler draughts. Vortex generators increase the heat transfer coefficient in the mentioned area. Prepared CFD analysis does not include vortex generators in the domain because of limited available computing power. Therefore obtained heat load in the domain will be lower than measured in the experiment.

In the analysis of the result, two additional parameters are used. The first physical quantity is the magnitude of flue gas which is flowing through the first draught. It is defined as a product of velocity and density according to the definition (6).

$$\dot{m}_{eg, D_l} = F \cdot u_{eg,D_l} \cdot \rho_{eg,D_l} \tag{6}$$

The second value is a relative mass flow through the tubes located in the first draught which was defined according to the equation (7).

$$r_{\dot{m}, D_l} = \frac{\dot{m}_{eg,R_xD_l}}{\dot{m}_{eg, out}} \cdot 100\% \tag{7}$$

The mentioned value allows for showing what part of exhausts flows to the afterburning chamber with the omission of the first two draughts.

4. Results and discussion

Fig. 4 shows the temperature distribution of exhaust gas in the heating boiler for two analyzed levels of the heat load in the XY plane according to Fig. 3. The mentioned plane allows for showing differences of flow for all analyzed cases between free and limited stream which is directed to the afterburning chamber. Crucial parameters connected with the heating boiler work for all analyzed cases are collected in Table 4.

During the work with the nominal power, the limitation of flue gas flow into the afterburning chamber caused the reduction of temperature of exhaust gas at the outlet by 7 °C. It is caused by a flow path extension for a higher mass flow of fumes through the first and second draught. It is connected with a greater magnitude of convective heat transfer caused by a higher velocity of flue gas, which has a tremendous impact on the Reynolds number and in consequence for the Nusselt number in the mentioned area. The temperature difference between analyzed cases at the outlet from the domain has an impact on increasing heating power by 4.2%. Limitation of exhaust gasses flow into the afterburning chamber

Fig. 4. Temperature distribution of flue gas in the XY plane, a) unhampered flow for 30% of nominal power, b) limited flow for 30% of nominal power, c) unhampered flow for 100% of nominal power, d) limited flow for 100% of nominal power.

Table 3
Streams of working mediums at the inlet to the domain.

$\dot{Q}$ (kW)	$\dot{m}_{eg}$ (kg/s)	$\dot{m}_w$ (kg/s)
6	0.006	0.165
18	0.02	0.55

Table 4
Crucial parameters for exhaust gas flow through the heating boiler.

P_n (%)	30%		100%	
	a	b	a	b
$t_{eg,out}$ (°C)	138	107	228	221
$u_{max,eg}$ (m/s)	2.0	2.1	4.1	5.3
p_d (Pa)	2.82	2.62	7.63	12.2
$\dot{Q}$ (kW)	4.7	4.7	11.8	12.3

has a bigger impact on the temperature at the outlet from the domain in cases when the heat load is equal 30% of nominal power. Then it comes to degreasing of temperature at the outlet from the domain by 30 °C without visible changes in the heating power.

Velocity distribution obtained for analyzed cases located on the plane mentioned earlier is presented in Fig. 5. Obtained results for cases when flow through the duct 7 is free, inform that the whole stream of exhausts realized through directly to the afterburning chamber is performed by the left row of pipes of the last draught. This phenomenon is also confirmed in the analysis prepared for the definition of mass flow of flue gas in each tube of the third draught. The mentioned results are shown in Table 5. Collected data shows that independently from analyzed cases obtained for a lower stream of exhaust in a domain, in the part of the last draught reversed flow is occurring. Limitation of fumes flow into the afterburning chamber cause higher homogeneity of the exhaust gas stream in this area and reduces the temperature at the outlet of the domain. Obtained the same level of heating power for two analyzed cases is connected with increased exhaust cooling in the first two draughts for unhampered flow and direction of the higher stream of fumes back to the afterburning chamber.

When the heating boiler works with the nominal power, the phenomenon of reversed flow does not occur. It is connected with a higher mass flow of exhaust gas which has a big impact on pressure distribution in the third draught. However higher stream of fumes flows through pipes located in the central part of the boiler, which is the shortest way to the outlet in conjunction with low pressure of exhausts in this area. Limitation of exhaust gas flows through the duct connecting the combustion chamber with the afterburning chamber when heating boiler work with the nominal power also leads to higher homogeneity of the stream in every pipe creating the third draught. However higher stream of exhausts is still directed through the left line of pipes. The dominating impact for that phenomenon in both cases has eddy creation between connections with second and third draught in the area of the afterburning chamber.

Limitation of exhaust flow into the afterburning chamber changes the direction of the bigger stream of exhausts to the first and second draught of the boiler. Then a higher temperature of flue gas is present in this area. Increasing the temperature difference between working mediums cause the rising amount of heat transferred between working mediums. Also, a big impact on that phenomenon has the increased velocity of a flow according to the Reynolds number. Restriction of the flue gas flow to the afterburning chamber does not cause intense changes in maximum velocity for lower analyzed heat load of the heating device. In connection to the above does not come to an increase of a pressure drop in the domain. When the heating boiler works with the nominal power, limitation of a cross-section of duct 7 causes an increase of maximum velocity of exhaust gas by 30%, which results in additional pressure drop of the flue stream. Pressure drop increment after the limitation of fumes flow is increased by 4.6 Pa which is equal to 60% more than in cases when exhaust flow is unhampered.
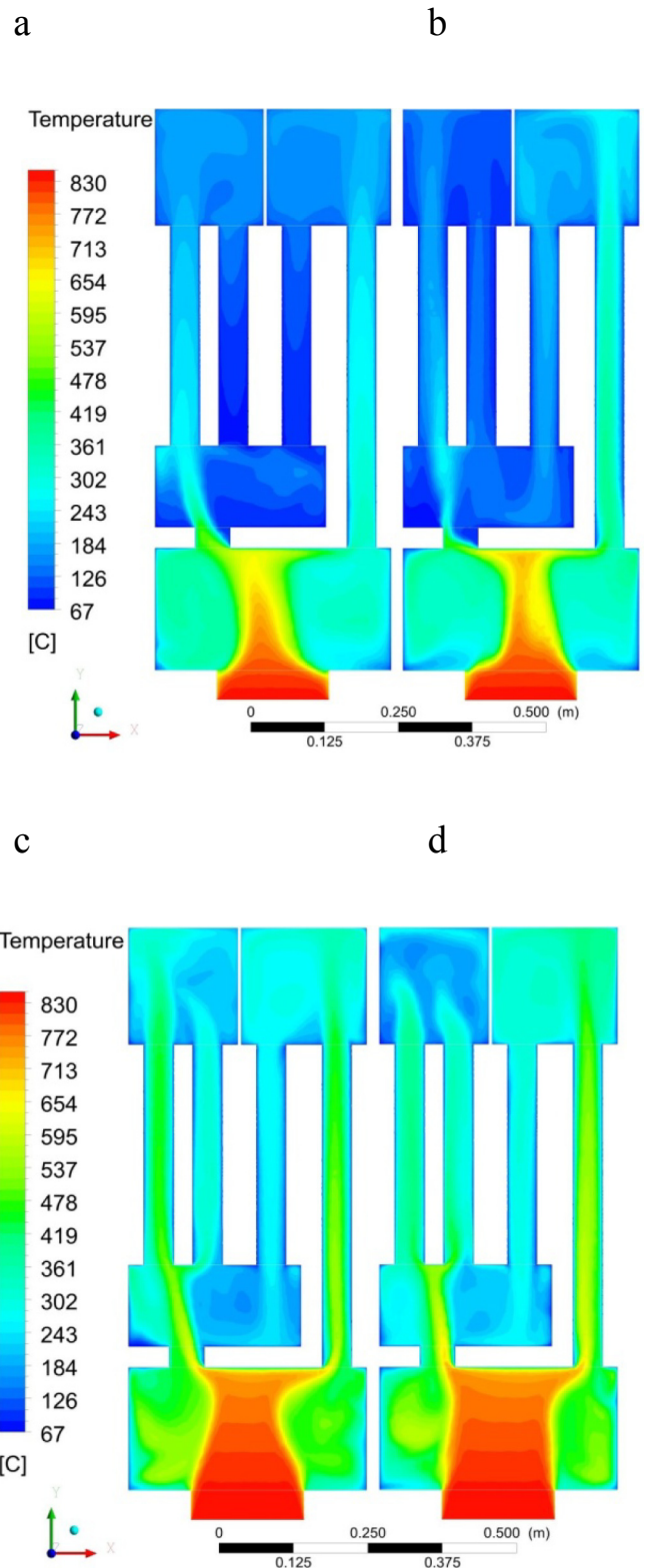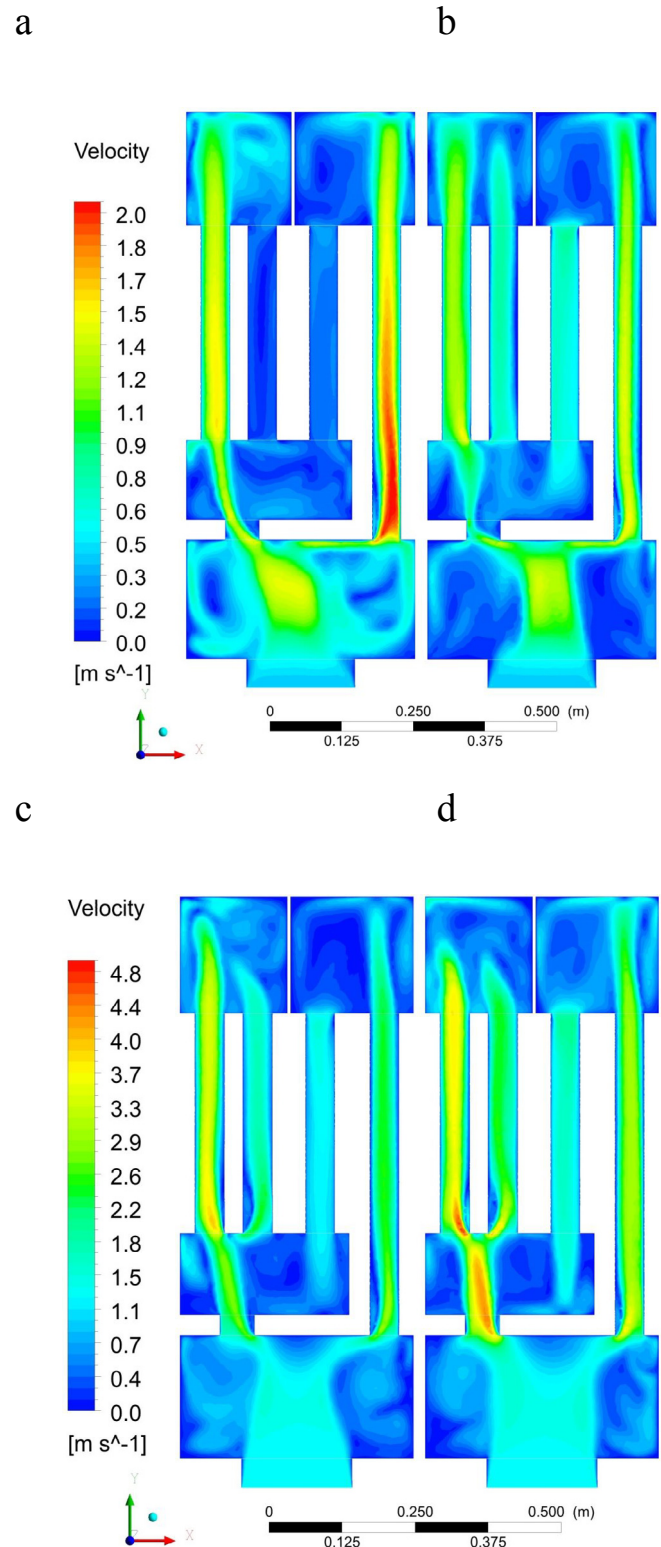

Fig. 5. Velocity distribution of flue gas in the XY plane, a) unhampered flow for 30% of nominal power, b) limited flow for 30% of nominal power, c) unhampered flow for 100% of nominal power, d) limited flow for 100% of nominal power.

Fig. 6 shows an amount of exhaust flow through the first draught on the YZ plane (according to the scheme of the boiler) located in the cross-section of the first draught. The percentage of exhausts mass flow divided into respective tubes is presented in

Table 5
Distribution of mass flow obtained for each pipe in the third draught.

P_n (%)	30%			
case	a		b	
row	line			
	C1	C2	C1	C2
R1	30.8%	**−7.3%**	**−6.0%**	**−5.3%**
R2	34.7%	**−6.6%**	**−6.0%**	14.7%
R3	36.8%	**−5.1%**	34.6%	20.9%
R4	23.6%	**−6.9%**	30.8%	16.3%
P_n (%)	100%			
row	column			
	C1	C2	C1	C2
R1	10.7%	8.1%	7.9%	7.6%
R2	17.5%	11.4%	11.9%	10.7%
R3	18.0%	11.5%	21.1%	14.6%
R4	13.0%	9.7%	14.1%	12.0%

Table 6. Mentioned value is obtained by division of mass flow for each tube of mentioned draught divided by the total mass flow of exhaust gas flow at the outlet from the domain. The character of flow through the first draught for the unhampered flow is much different depending on the heat load of the heating device. When the boiler works with the minimal level of the heat load exhausts are directed to the reversing chamber which connects first and second draught only by two internal two tubes of the first draught. Two external pipes are responsible for occurring of reversed flow which directs fumes back to the combustion chamber. It is caused by eddies generated inside the reversing chamber, located above to the outlet from external pipes in the first draught. Then only 31.4% of exhaust flows through the first draught. Restriction of flow to the afterburning chamber caused that almost 90% of exhaust gas flow through this part. A higher amount of exhaust gas is received equally by all ducts located in the mentioned area. The combustion process for the minimal power of the heating device does not generate a large amount of exhaust gas stream. A limited amount of exhausts could easily move through the available space in the first draught equally filling each duct. Then do not come to the pressure drop increases.

When the heating boiler operates with the nominal power a higher volume of exhausts is present in the domain. It is connected with a higher partial pressure of elementary compounds of exhaust gas. The effects are highly visible in the resistance of flow according to the Bernoulli equation. Limitation of exhaust gases flows through the duct connecting the combustion chamber with the afterburning chamber causes, that about 37% of fumes are transported through the first draught of the heating boiler. The distribution of exhaust gas in each of the four pipes is uniform. The limitation of a flow to the afterburning chamber caused a higher stream of fumes has to appear in the first draught. Then 51% of the overall stream of exhaust gas flows through this area. It is the main reason for the increased pressure drop in the domain.

5. Conclusions

Small heating boilers used in the domestic applications work in a wide range of heat load. For the most part of the year, boilers work with the heating power close to 30% of the nominal heat load.

The character of a flue gas flow through the heat exchanger chamber strongly depends on the heat load of the heating device according to the number of exhausts present in the domain. The amount of fumes in the heat exchanger chamber has the main
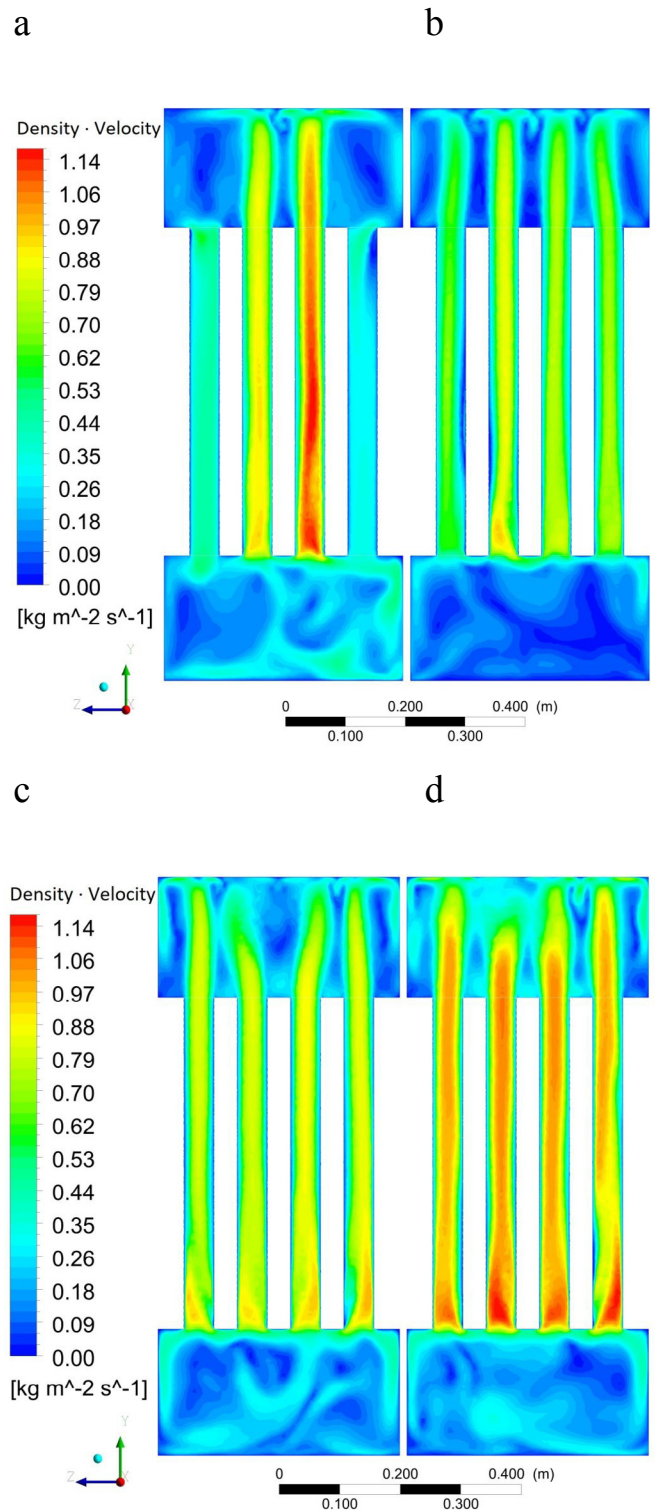
Fig. 6. Distribution of amount of exhaust flow through the first draught a) unhampered flow for 30% of nominal power, b) limited flow for 30% of nominal power, c) unhampered flow for 100% of nominal power, d) limited flow for 100% of nominal power.

influence on a pressure drop of exhaust gas between the combustion chamber and the flue of the boiler. It also affects the eddy generation in the domain, which has to dominate influence for irregular character of flow between each tubes forming heating

Table 6
Distribution of exhaust mass flow obtained for each pipe in the first draught referred to mass flow at the outlet from the domain.

P_n (%)	30%		100%	
row	case			
	a	b	c	d
R1	**−16.1%**	18.6%	8.9%	12.6%
R2	28.1%	25.2%	9.1%	13.3%
R3	31.5%	22.5%	9.7%	13.1%
R4	**−12.0%**	21.4%	9.1%	12.3%

boiler draughts.

Appropriate division of exhaust gases stream between ducts of the heating boiler allows achieving optimal parameters of flow for each level of the heat load. Implementation of a regulation system responsible for controlling of amount of exhaust gas developed into the afterburning chamber allows us to achieve fractional influence for a pressure drop with preserving of the high efficiency of heating boiler work, depends on the heat load of the heating device.

Declaration of competing interest

The authors report no conflicts of interest. The authors alone are responsible for the content and writing of this article.
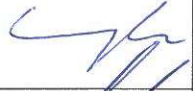
Acknowledgments

References

[1] Stala-Szlugaj K. Trends in the consumption of hard coal in Polish households compared to EU households. Miner Resour Manag 2016;32:5−22. https://doi.org/10.1515/gospo-2016-0024.

[2] Kerimray A, Rojas-Solórzano L, Amouei Torkmahalleh M, Hopke PK, Ó Gallachóir BP. Coal use for residential heating: patterns, health implications and lessons learned. Energy Sustain Dev 2017;40:19−30. https://doi.org/10.1016/j.esd.2017.05.005.

[3] Commision Regulation (EU). 2015/1189 - of 28 April 2015 - implementing Directive 2009/125/EC of the European Parliament and of the Council with regard to ecodesign requirements for solid fuel boilers. 2015.

[4] Directive 2009/125/EC of the European Parliament and of the Council of 21 October 2009 establishing a framework for the setting of ecodesign requirements for energy-related products. 2009.

[5] Zhang X, Yuan J, Chen Z, Tian Z, Wang J. A dynamic heat transfer model to estimate the flue gas temperature in the horizontal flue of the coal-fired utility boiler. Appl Therm Eng 2018;135:368−78. https://doi.org/10.1016/j.applthermaleng.2018.02.067.

[6] Yang J-H, Kim J-EA, Hong J, Kim M, Ryu C, Kim YJ, et al. Effects of detailed operating parameters on combustion in two 500-MWe coal-fired boilers of an identical design. Fuel 2015;144:145−56. https://doi.org/10.1016/j.fuel.2014.12.017.

[7] Laubscher R, Rousseau P. Numerical investigation into the effect of burner swirl direction on furnace and superheater heat absorption for a 620 MWe opposing wall-fired pulverized coal boiler. Int J Heat Mass Tran 2019:506−22. https://doi.org/10.1016/j.ijheatmasstransfer.2019.03.150.

[8] Madejski P. Numerical study of a large-scale pulverized coal-fired boiler operation using CFD modeling based on the probability density function method. Appl Therm Eng 2018;145:352−63. https://doi.org/10.1016/j.applthermaleng.2018.09.004.

[9] Wang H, Zhang C, Liu X. Heat transfer calculation methods in three-dimensional CFD model for pulverized coal-fired boilers. Appl Therm Eng 2019:114633. https://doi.org/10.1016/j.applthermaleng.2019.114633.

[10] Maakala V, Järvinen M, Vuorinen V. Optimizing the heat transfer performance of the recovery boiler superheaters using simulated annealing, surrogate modeling, and computational fluid dynamics. Energy 2018;160:361−77. https://doi.org/10.1016/j.energy.2018.07.002.

[11] Madejski P, Taler D, Taler J. Modeling of transient operation of steam superheater in CFB boiler. Energy 2019;182:965−74. https://doi.org/10.1016/j.energy.2019.06.093.

[12] Taler D, Taler J. Simplified analysis of radiation heat exchange in boiler

[13] Taler J, Taler D, Kaczmarski K, Dzierwa P, Trojan M, Sobota T. Monitoring of thermal stresses in pressure components based on the wall temperature measurement. Energy 2018;160:500−19. https://doi.org/10.1016/j.energy.2018.07.010.

[14] Blaszczuk A, Pogorzelec M, Shimizu T. Heat transfer characteristics in a large-scale bubbling fluidized bed with immersed horizontal tube bundles. Energy 2018;162:10−9. https://doi.org/10.1016/j.energy.2018.08.008.

[15] Blaszczuk A, Nowak W. The impact of bed temperature on heat transfer characteristic between flui-dized bed and vertical rifled tubes. J Therm Sci 2016;25:476−83. https://doi.org/10.1007/s11630-016-0887-2.

[16] Rajh B, Yin C, Samec N, Hribersek M, Kokalj F, Zadravec M. Advanced CFD modelling of air and recycled flue gas staging in a waste wood-fired grate boiler for higher combustion efficiency and greater environmental benefits. J Environ Manag 2018;218:200−8. https://doi.org/10.1016/j.jenvman.2018.04.030.

[17] Bermúdez CA, Porteiro J, Varela LG, Chapela S, Patiño D. Three-dimensional CFD simulation of a large-scale grate-fired biomass furnace. Fuel Process Technol 2020;198. https://doi.org/10.1016/j.fuproc.2019.106219.

[18] Gu J, Zhang Y, Wu Y, Li Z, Tang G, Wang Q, et al. Numerical study of flow and heat transfer of supercritical water in rifled tubes heated by one side. Appl Therm Eng 2018;142:610−21. https://doi.org/10.1016/j.applthermaleng.2018.07.017.

[19] Li Z, Wu Y, Tang G, Zhang D, Lu J. Comparison between heat transfer to supercritical water in a smooth tube and in an internally ribbed tube. Int J Heat Mass Tran 2015;84:529−41. https://doi.org/10.1016/j.ijheatmasstransfer.2015.01.047.

[20] Barma MC, Saidur R, Rahman SMA, Allouhi A, Akash BA, Sait SM. A review on boilers energy use, energy savings, and emissions reductions. Renew Sustain Energy Rev 2017;79:970−83. https://doi.org/10.1016/j.rser.2017.05.187.

[21] Gómez MAA, Martín R, Chapela S, Porteiro J. Steady CFD combustion modeling for biomass boilers: an application to the study of the exhaust gas recirculation performance. Energy Convers Manag 2019;179:91−103. https://doi.org/10.1016/j.enconman.2018.10.052.

[22] Gómez MA, Porteiro J, Patiño D, Míguez JL. Fast-solving thermally thick model of biomass particles embedded in a CFD code for the simulation of fixed-bed burners. Energy Convers Manag 2015;105:30−44. https://doi.org/10.1016/j.enconman.2015.07.059.

[23] Gómez MA, Porteiro J, de la Cuesta D, Patiño D, Míguez JL. Numerical simulation of the combustion process of a pellet-drop-feed boiler. Fuel 2016;184:987−99. https://doi.org/10.1016/j.fuel.2015.11.082.

[24] Chapela S, Porteiro J, Gómez MA, Patiño D, Míguez JL. Comprehensive CFD modeling of the ash deposition in a biomass packed bed burner. Fuel 2018;234:1099−122. https://doi.org/10.1016/j.fuel.2018.07.121.

[25] Scharler R, Gruber T, Ehrenhöfer A, Kelz J, Bardar RM, Bauer T, et al. Transient CFD simulation of wood log combustion in stoves. Renew Energy 2020;145:651−62. https://doi.org/10.1016/j.renene.2019.06.053.

[26] Wiese J, Wissing F, Höhner D, Wirtz S, Scherer V, Ley U, et al. DEM/CFD modeling of the fuel conversion in a pellet stove. Fuel Process Technol 2016;152:223−39. https://doi.org/10.1016/j.fuproc.2016.06.005.

[27] Chaney J, Liu H, Li J. An overview of CFD modelling of small-scale fixed-bed biomass pellet boilers with preliminary results from a simplified approach. Energy Convers Manag 2012;63:149−56. https://doi.org/10.1016/j.enconman.2012.01.036.

[28] Khodaei H, Al-Abdeli YM, Guzzomi F, Yeoh GH. An overview of processes and considerations in the modelling of fixed-bed biomass combustion. Energy 2015;88:946−72. https://doi.org/10.1016/j.energy.2015.05.099.

[29] Nosek R, Jandacka J, Szlek A. Transaction on mechanical power and process simulation of coal combustion in small boiler. Global J Technol Optim 2011;2:121−9.

[30] Ryfa A, Buczynski R, Chabinski M, Szlek A, Bialecki RA. Decoupled numerical simulation of a solid fuel fired retort boiler. Appl Therm Eng 2014;73:794−804. https://doi.org/10.1016/j.applthermaleng.2014.08.029.

[31] Buczynski RB, Weber R, Szlek A, Nosek R. Time-dependent combustion of solid fuels in a fixed-bed: measurements and mathematical modeling. Energy Fuels 2012;26:4767−74. https://doi.org/10.1021/ef300676r.

[32] Athanasios N, Nikolaos N, Nikolaos M, Panagiotis G, Kakaras E. Optimization of a log wood boiler through CFD simulation methods. Fuel Process Technol 2015;137:75−92. https://doi.org/10.1016/j.fuproc.2015.04.010.

[33] Morán JC, Tabarés JL, Granada E, Porteiro J, López González LM. Effect of different configurations on small pellet combustion systems. Energy Sources, Part A Recover Util Environ Eff 2006;28:1135−48. https://doi.org/10.1080/009083190910505.

[34] Urbaniak R, Bartoszewicz J, Judt W. Aanalysis of the possibilities of application of numerical methods in the improvement of the operating efficiency of low-power boilers. Heat Tran Res 2018;49:675−83. https://doi.org/10.1615/HeatTransRes.2018019827.

[35] Rezeau A, Díez LI, Royo J, Díaz-Ramírez M. Efficient diagnosis of grate-fired biomass boilers by a simplified CFD-based approach. Fuel Process Technol 2018;171:318−29. https://doi.org/10.1016/j.fuproc.2017.11.024.

[36] Judt W, Bartoszewicz J. Analysis of fluid flow and heat transfer phenomenon in a modular heat exchanger. Heat Tran Eng 2019:1−14. https://doi.org/10.1080/01457632.2019.1699291. in press.

[37] Ziegler B, Mosiężny J, Czyżewski P. Unsteady CHT analysis of a solid state,

superheaters. Heat Tran Eng 2009;30:661−9. https://doi.org/10.1080/01457630802659953.

sensible heat storage for PHES system. Int J Numer Methods Heat Fluid Flow 2019. https://doi.org/10.1108/HFF-11-2018-0701.

[38] Joachimiak M, Joachimiak D, Ciałkowski M, Małdziński L, Okoniewicz P, Ostrowska K. Analysis of the heat transfer for processes of the cylinder heating in the heat-treating furnace on the basis of solving the inverse problem. Int J Therm Sci 2019;145. https://doi.org/10.1016/j.ijthermalsci.2019.105985.

[39] Jones FE, Harris GL. ITS-90 density of water formulation for volumetric standards calibration. J Res Natl Inst Stand Technol 2012;97:335–40. https://doi.org/10.6028/jres.097.013.

[40] Barichello LB, Siewert CE. A discrete-ordinates solution for a non-grey model with complete frequency redistribution. J Quant Spectrosc Radiat Transf 1999;62:665–75. https://doi.org/10.1016/S0022-4073(98)00096-X.

[41] Wilcox DC. Formulation of the k-ω turbulence model revisited. AIAA J 2008;46:2823–38. https://doi.org/10.2514/1.36541.

[42] Tuliszka E. Technical thermodynamics. Warszawa: National Scientific Publishing; 1978.

[43] Pudlik W. Thermodynamic. third ed. Gdańsk: Gdansk University of Technology Publishing House; 2011.

[44] Junga R, Wzorek M, Kaszubska M. Technical and environmental performance of 10 kW understocker boiler during combustion of biomass and conventional fuels. E3S Web Conf 2017;19:01009. https://doi.org/10.1051/e3sconf/20171901009.

[45] Polák M, Neuberger P. The optimisation of biomass combustion. Infrastruct Ecol Rural Areas 2008:63–70.

[46] de Souza-Santos ML. Solid fuels combustion and gasification: modeling, simulation, and equipment operations. second ed. CRC Press; 2010. https://doi.org/10.1201/9781420047509.

Poznań, 16.06.2020

Oświadczenie o wkładzie poszczególnych autorów w postanie publikacji naukowej

Wojciech Judt, Bartosz Ciupek, Rafał Urbaniak, Numerical study of a heat transfer process in a low power heating boiler equipped with afterburning chamber, Energy - 2020, vol. 196, DOI: 10.1016/j.energy.2020.117093

Lp.	Imię i nazwisko	Włożony nakład pracy	Udział %	Podpis
1.	Wojciech Judt	Przegląd literatury, przygotowanie siatki obliczeniowej, realizacja obliczeń numerycznych, redakcja tekstu publikacji, przygotowanie rysunków i tabel.	85%	
2.	Bartosz Ciupek	Zebranie danych wejściowych koniecznych do przygotowania warunków brzegowych w modelu.	10%	
3.	Rafał Urbaniak	Wsparcie merytoryczne, wsparcie dotyczące syntezy rezultatów.	5%	

Article

Numerical and Experimental Analysis of Heat Transfer for Solid Fuels Combustion in Fixed Bed Conditions

Wojciech Judt

Department of Fuels and Renewable Energy, Faculty of Environmental Engineering and Energy, Institute of Thermal Engineering, Poznan University of Technology, 60-965 Poznan, Poland; wojciech.judt@put.poznan.pl; Tel.: +48-61-665-23-31

Abstract: The paper concerns the analysis of the heat transfer process that occurred during solid fuel burning in fixed bed conditions. The subject of the analysis is a cylindrical combustion chamber with an output of 12 kW heating power equipped with a retort burner for hard coal and biomass combustion. During the research, a numerical and experimental study is performed. The analysis is prepared for various heat load of the combustion chamber, which allowed for the reconstruction of real working conditions for heating devices working with solid fuels combustion. The temperature distribution obtained by the experimental way is compared with results of the numerical modeling. Local distribution of principal heat transfer magnitudes like a heat flux density and a heat transfer coefficient that occurred on the sidewall of the combustion chamber is analyzed. The analysis showed, that the participation of convection and radiation in the overall heat transfer process has resulted from the heat load of the heating device. Research results may be used for improving an analytical approach of design process taking place for domestic and industrial combustion chambers.

Keywords: solid fuels; fixed bed; combustion; heat transfer; heat load; CFD; modeling; experimental analysis

---

1. Introduction

Solid fuel combustion is one of the main sources of thermal energy used for heating purposes by the individual and commercial sector in Poland. According to data from 2018 [1], 35.7% of Polish households were heated by heating devices using solid fuels. Heat provided by thermal plants was delivered to 40.4% of Polish households. The Energy Regulatory Office in Poland reported [2] that in 2019 solid fuel combustion was responsible for 80.2% of the heat generated by the commercial sector. Moreover, 9.2% of the heat generated by the commercial sector originated from solid biomass burning. Nowadays changes in thinking about the environment cause the replacement of fossil fuel by renewable fuels like biomass. From one year to another the amount of heat generated by fossil fuel burning decreases and is replaced by different types of renewable sources of energy. Solid biomass share in energy production from renewable sources in Poland was equal to 67.9% in 2017. European Union average for the mentioned magnitude was 42% in the same year [3]. This means that solid fuel burning for some time will be still the main source of heat generation.

One of the main methods for solid fuel combustion for domestic and industrial boilers is realized in fixed bed conditions. Computational Fluid Dynamic (CFD) modeling is often used to simulate packed bed burning. Fixed bed combustion modeling can be divided into two main groups. The first group is concerned with a small-scale, when a combustion process is realized in a range of heating power equal from over a dozen to tens of kilowatts. The mentioned group may belong to one-dimensional models

focused on the phenomena that occurred during combustion of a single grain of a fuel. The second one deals with a huge scale, where obtained heating power from fixed bed combustion equals from few to tens megawatts.

Scharler et al. [4] raised the issue of how the low power log stove burning modeling focused on CO concentration in the flue gas. Wiese et al. [5] have been dealing with a transient simulation of pellet burning with the application of a discrete element model in CFD calculations for a 13 kW stove. Mehrabian et al. [6] and Gomez et al. [7] are concerned with numerical modeling of the thermally thick approach of biomass burning. Gomez et al. [8] also have been using the mentioned approach for a 27 kW domestic boiler working conditions modeling. In other works [9,10] he also modeled emissions of harmful compounds during fixed-bed biomass burning in a 60 kW domestic boiler by steady and transient analysis. Similar transient modeling connected with the analysis of the chemical composition of exhausts was realized by Mehrabian et al. [11] in a laboratory-scale biomass fixed bed batch. Collazo et al. [12] also have been working on a transient simulation of a pellet wood burning for a laboratory combustor. He was targeting a temperature distribution at different points in the bed. Researchers from Clausthal University of Technology and Silesian University of Technology [13,14] were involved in numerical modeling of coal burning in small-scale retort boilers. They analyzed possibilities of the perfecting of domestic boiler construction in terms of pollution limitation and optimization of temperature distribution inside a combustion chamber. Chaney et al. [15] modeled a 50 kW packed bed biomass boiler in terms of investigating the optimization of the combustion performance and NO_x emissions. A new approach of packed bed biomass burning was presented by Chapela et al. [16]. His Eulerian-fouling model is computationally less expensive and shows a better response to the experimental data.

Tu et al. [17,18] modeled a 32 MW woodchip-fired grate boiler work with different operating conditions directed on NO_x reduction mechanisms. Silva et al. [19] were concerned about 34.6 MW biomass grate-fired boiler modeling. He was focused on an analysis of temperature, velocity, and species field of exhaust gas within a boiler, which provided to the optimization of the burning process. Moving grate biomass boilers models realized in two different scales (250 kW and 4 MW) were analyzed by Rezeau et al. [20] and Bermúdez et al. [21] in terms of composition and temperature distribution of flue gas. Klason et al. [22] analyzed a radiation heat transfer process in two various scales (10 kW and 50 MW) during biomass burning in fixed bed furnaces. He has obtained a gas temperature profile inside the combustion chamber located above a fixed bed with the assumption of constant temperature for furnace walls. Moreover, he investigated the accuracy of a solution for different radiation heat transfer models.

The abovementioned research connected with the fixed bed modeling is concerned mainly with the emission of harmful compounds during solid fuel combustion. Moreover, there has been raised the issue of the temperature distribution occurring in the combustion chamber and inside a packed bed of fuel. Researchers do not relate achieved results of temperature distribution to prepare an in-depth analysis of the heat transfer process in modeled heating devices. The issue of heat transfer phenomenon occurring in a wall neighborhood and free-room of a combustion chamber during fixed-bed combustion still has not been deeply recognized like it is realized in other types of thermal devices used for different industrial applications, like heat treatment furnaces [23–25], heat storage systems [26–28], or heat exchangers [29–31]. So far available results concerned about the packed bed burning assumed a temperature of combustion chamber walls as a boundary condition. Then a constant wall temperature was present for each wall of the combustion chamber or separately, at particular elements of modeled furnaces. Computational grids used in computational models were suitable for free-room analysis like bulk gas temperature and chemical composition. Grids used in the previous research were not capable of heat transfer analysis that occurred on combustion chamber walls. This was caused by the size of grid elements located near the combustion chamber wall (dimensionless wall distance $y^+ \gg 1$) being too high to obtain an appropriate solution of heat flux at the wall of the combustion chamber. Moreover, so far available packed bed burning models used wall functions for simulating the near-wall

region (k-ε model of turbulence). The mentioned approach does not show sufficient accuracy for viable modeling of conditions that occurred near combustion chamber walls which are necessary for modeling a heat transfer process.

2. Materials and Methods

2.1. Initial Assumptions

The author analyzed a case when a combustion process has occurred inside fixed bed conditions. Conducted research was divided into two main parts. Firstly, an experimental analysis was prepared. The second part has relied on the preparation of a numerical model. The combustion process of two types of solid fuels was analyzed. It was hard coal and wood biomass in a pellet form. Proximate and ultimate analysis of fuels used during the research is presented in Table 1. The author analyzed the work of the test stand with two levels of heating power. It was 50% and 100% of the nominal heat load. The test stand used during the conducted research is capable of transferring 12 kW of heat to the cooling water during nominal work. The proposed research is concerned with the investigation of the heat transfer phenomenon that occurred in a near-wall region of the combustion chamber. Application of various types of fuels and levels of a heat load allowed for an analysis occurring during real exploitation in the whole range of heating device working conditions.

Table 1. Proximate and ultimate analysis of used fuels.

Parameter	Hard Coal	Biomass
moisture (%)	5.8	5
ash (%)	3.4	0.4
volatile (%)	31.5	77
carbon (%)	75.6	46.6
hydrogen (%)	4.2	5.5
oxygen (%)	9.3	40.9
nitrogen (%)	1.4	1.2
sulphur (%)	0.4	0.4
LCV (MJ/kg)	29	18

2.2. Experimental Research

A cylindrical combustion chamber is used in the experimental part of the research. The scheme of the test stand is present in Figure 1. The heat generated from fuel combustion is transferred to the cooling water located along the cylinder side and the top surface, where a water jacket is present. A retort burner was used to form a packed bed during the research. Solid fuel with the right grain size is developed into a combustion process by a screw feeder, pushing them up. Air is supplied to the combustion process utilizing a fan. Primary air is delivered directly to the packed bed flowing through the layers of fuel.

The mentioned type of burner brings out a flame above the fuel bed. At a distance of 15 cm above the top edge of the burner, a deflector is mounted. This element is a disc-shaped cast iron element, whose main task is the dispersion of flames in the whole volume of the combustion chamber. The effect is visible in a more uniform temperature distribution inside the combustion chamber.

The test stand allows for gas temperature measurement inside the combustion chamber through 14 holes distributed every 10 cm along with chamber height according to Figure 1. The first hole was located 13 cm from the top plane of the burner (two centimeters below the bottom edge of the deflector). Measurements were done in 6 points for every plane, where the first point was present in the chamber axis. Other points were located every 5 cm in the wall direction. Because of the axisymmetric shape of the chamber, measurement was prepared only for half of the chamber. Gas temperature measurement was realized by K type thermocouples. The mentioned type of temperature detectors allows for temperature measurements down to 1200 °C.
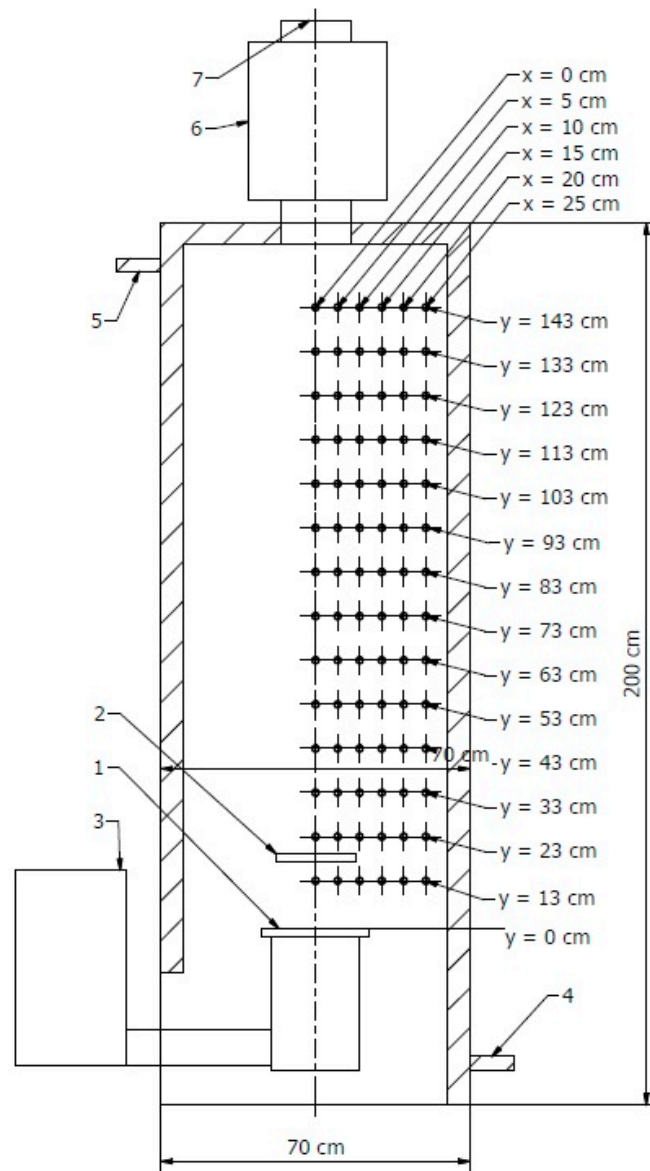
Figure 1. Scheme of a cylindrical chamber with marked measurement points used during the experiment, 1—retort feeder, 2—deflector, 3—fuel tray, 4—water inlet, 5—water outlet, 6—insulated measurement duct, 7—flue gas outlet to the chimney.

During the experiment, exhausts gas composition was measured by the application of the Testo 350 gas analyzer. It allowed for combustion process control and was also used for quality assessment of results obtained during numerical calculations. Oxygen and carbon dioxide content in exhausts was analyzed for that purpose. Assignation of the amount of mentioned gases in exhausts allowed for validation of exhaust composition obtained during numerical analysis. A mass of particular matter present in exhausts was measured by the Testo 380 soot analyzer. The mentioned parameter was necessary for the proper determination of the exhaust gas absorption coefficient, which is crucial given the influence of a radiation heat transfer.

Heat received from the burning process is transported to a heat exchanger according to a scheme showed in Figure 2.
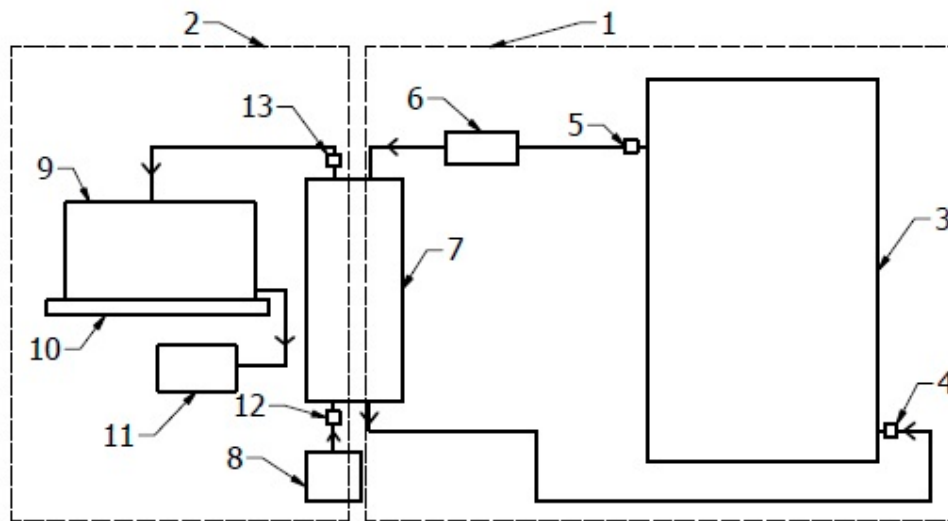
Figure 2. Scheme of a cooling system, 1—first circuit of water flow, 2—second circuit of water flow, 3—combustion chamber, 4—PT100 measurement point at inlet to test stand, 5—PT100 measurement point at outlet from test stand, 6—vane flow meter, 7—plate heat exchanger, 8—cold water supply, 9—bath, 10—scale, 11—hot water drain, 12—PT100 measurement point at inlet to the heat exchanger for water in secondary circuit, 13—PT100 measurement point at outlet from the heat exchanger for water in secondary circuit.

Applied installation is composed of two circuits. Water which is located in the first circuit transport heat between the test stand and the plate heat exchanger, where the mentioned heat is received by a second circuit. The temperature of cooling water was analyzed for the determination of the heating power of the test stand during the experiment. It was obtained by the application of PT100 detectors at the water inlet and outlet (points 4 and 5). Mass flow of water used for test stand cooling was measured by a heat meter equipped with a vane flow meter. The second circuit is equipped with an additional heating power check system. Water supply 8 supplied cold water to the plate heat exchanger. After heating water is directed into a bath located on a scale. The temperature of water in the second circuit is also measured by PT100 detectors (points 12 and 13). The mass flow of water flowing through the second circuit is determined based on a weight of water measured by a scale at a certain time of measurement.

2.3. Numerical Modeling

2.3.1. Domain and Mesh

Numerical analysis of solid fuel combustion inside a fixed bed is modeled in the ANSYS Fluent software (Ansys Inc., Canonsburg, PA, USA). Numerical calculations are realized in a steady state due to high thermal inertia during heating boiler work. Results obtained during experimental research after averaging were compared with a steady-state numerical solution. Calculations were made for one-fourth part of the cylindrical combustion chamber used over the experiment due to the symmetry of the domain. The geometrical model used in numerical analysis is shown in Figure 3.
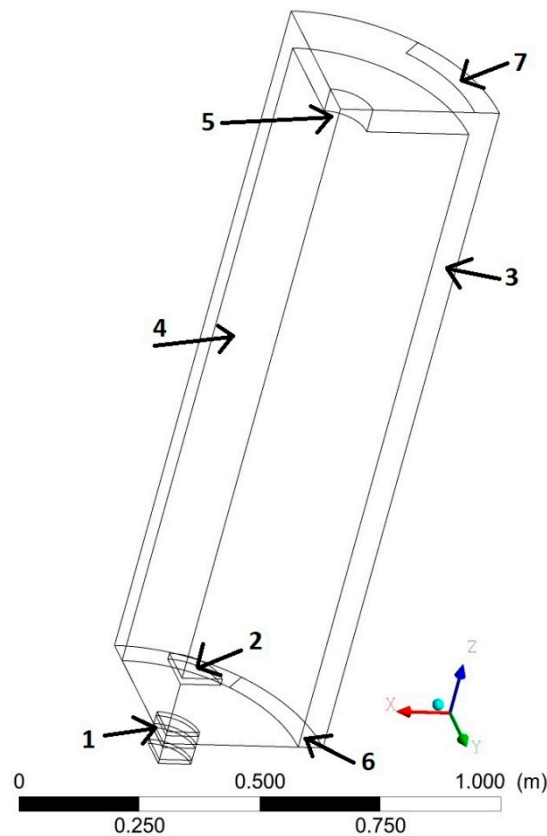
Figure 3. Overview on a computational domain, 1—volume of fixed bed, 2—deflector, 3—water jacket, 4—combustion chamber, 5—exhaust gas outlet, 6—cooling water inlet, 7—cooling water outlet.

Calculations are prepared on a structural, hexagonal grid. The mentioned mesh was prepared in the Numeca IGG software. Optimal mesh parameters originate from the results of realized preliminary calculations. The crucial specification of the finally used grid is presented in Table 2. Dimensions of the numerical domain are consistent with a test stand used during the experimental part of the research. Dimensionless wall distance parameter y^+ has a big impact on a heat flux calculation during heat transfer modeling between exhaust gas and cooling water. An appropriate number of elements in applied mesh results from a necessity of ensuring the mentioned parameter close to 1. Then the first layer of grid located near to heat transfer wall for both fluids taking part in conjugate heat transfer allows for the calculation of a heat flux value complied with experimental analysis.

Table 2. Parameters of the grid used in numerical calculations.

Parameter	Value
number of cells	2.9 M
y^+	≈ 1
minimum orthogonal quality	0.82
maximum skewness	0.39

2.3.2. Setup

A discrete phase model is used for packed bed modeling. A solid fuel fixed bed is modeled by spherical particles that are tightly packed in the bottom part of the domain according to Figure 3. The size of particles is uniform and complies with the average size of fuels used during the experimental part. The contact of discrete particles to burner walls and relative to each other is modeled by the discrete element model. The mentioned model applies a Hertz problem basing on the Young Modulus

and Poisson Ratio of materials coming into mutual contact. Fuel located inside the bed is subjected to heat and mass transfer phenomena. Five successive laws are implemented for modeling of thermal transformation of the fuel (inert heating, vaporization, boiling, devolatilization, and surface combustion). Inert heating is applied while the particle temperature is less than the vaporization temperature. The mentioned process occurs also after boiling, but when the devolatilization temperature has not been reached. It is also present after the surface combustion process, where it comes to the heating of non-flammable parts of fuel. Vaporization concerns moisture content in fuel and is present when the temperature of the droplet reaches the vaporization temperature and continues until the droplet reaches the boiling point. After reaching a boiling temperature a boiling process has been started and will be continued until a moisture fraction is present in the discrete phase. Devolatization is based on a single rate model which assumes that the rate of devolatilization is the first-order dependent on the number of volatiles remaining in the particle. After the volatile component is completely evolved, a surface reaction begins which consumes the combustible fraction of the particle [32].

A pressure drop occurred during gas flow through the fixed bed is modeled as a porous zone. A momentum source term composed of viscous and inertial loss terms is added to the standard fluid flow equations set being solved during numerical calculations. Gas flow through the packed bed is modeled as laminar. Pressure drop obtained during flow through the packed bed is calculated by the Carman-Kozeny Equation (1).

$$\frac{\Delta p}{L} = -\frac{150 \mu}{D_p^2} \frac{(1-\varepsilon)^2}{\varepsilon^3} v_\propto \tag{1}$$

Viscous and inertial resistance magnitudes are used for the definition of source term applied during porous zone modeling. Viscous resistance is defined by inverse absolute permeability 1/k which is defined according to Equation (2). Inertial resistance is defined by inertial loss coefficient C_2, which is defined as in Equation (3) [32].

$$k = \frac{D_p^2}{150} \frac{\varepsilon^3}{(1-\varepsilon)^2} \tag{2}$$

$$C_2 = \frac{3.5}{D_p} \frac{(1-\varepsilon)}{\varepsilon^3} \tag{3}$$

The numerical model of solid fuel combustion is based on fast chemistry modeling. Chemical reactions are modeled by the application of species transport equations. Reaction rates are shaped by the Eddy Dissipation Model (EDM) and are dependent on occurring turbulent fluctuations. Two steps of the volumetric reaction mechanism are implemented for volatile burning modeling. EDM assumed that chemical kinetic rates are considerably faster than rates of turbulent mixing. Then turbulent mixing is responsible for the reaction rate-limiting process [33].

A Reynolds-stress model (RSM) is responsible for the effects of turbulence modeling during calculations. Results obtained by the RSM model are much closer to the experimental validation relative to the utilization of k-ε or k-ω SST models, which are popularly used in industrial CFD applications.

Radiation heat transfer is modeled by a Discrete Ordinates (DO) model. The considered model solves a radiation heat transfer equation for a finite number of discrete solid angles, which are associated with a vector $\vec{s}$ located in the global coordinate system. Calculations are being done for a three-dimensional domain where 8 octants are solved. The number of control angles that are used for discretization of each octant in the angular space is defined by Θ and Φ divisions (respectively polar and azimuthal angle measured in the global coordinate system). The numerical model takes into account 72 directions of vector $\vec{s}$ due to the application of three Θ and Φ divisions [34].

The absorption coefficient for exhaust gas is calculated as a sum of the absorption coefficient obtained for a pure gas and a soot fraction included in the mixture. The absorption coefficient that occurred for a

pure gas is calculated by a weighted sum of gray gases model (WSGGM) [35]. The influence of soot for a total absorption coefficient of exhausts is calculated based on Equation (4) [34],

$$a_s = b_1 \rho_s [1 + b_T(T - 2000)] \tag{4}$$

where ρ_s is a soot density, b_1 and b_T are coefficients obtained by S.S. Sazhin [36] based on data obtained from [37,38].

2.3.3. Boundary Conditions

Applied boundary conditions correspond to circumstances obtained during the experimental part of the research. A mass flow of cooling water at the inlet to the test stand results from the required levels of heating power for two analyzed levels of a load. The temperature of cooling water at the inlet to the computational domain arises from the heat load obtained in the cooling installation. The test stand during work with the nominal power can transfer about 12 kW of heat to the cooling water.

The mass flow of fuel provided as a discrete phase is calculated during analytical calculations. Analytical calculations are prepared based on own measurements of calorific value, moisture, ash, and volatile content in used fuels. Other data could not be obtained experimentally by the author, like the chemical composition of fuel originate from the database [39] for the most similar founded type of fuel. The mass flow of air delivered to the burning process is also calculated analytically. Calculations are prepared by taking into account an air excess factor based on experimental measurement of average oxygen content in the exhaust gas for each of the analyzed cases as in Equation (5).

$$\lambda = \frac{20.95\%}{20.95\% - O_{2,ave,mea}[\%]} \tag{5}$$

Analytical calculations were done with the assumption that the nominal power of the combustion process will equal 15 kW (3 kW intended for chimney loss and other wastes). Crucial parameters of boundary conditions at inlets to the computational domain are collected in Table 3. The mass flow used as boundary conditions is four times lower following real values because calculations are done for one-fourth of the real domain.

Table 3. Crucial physical magnitudes used as boundary conditions in the inlet to the numerical domain.

Fuel	Hard Coal		Biomass	
P_n (%)	50%	100%	50%	100%
$\dot{m}_w$ (kg/s)	50%	100%	50%	100%
$\dot{m}_f$ (kg/s)	5.7×10^{-2}	9.2×10^{-2}	5.7×10^{-2}	9.2×10^{-2}
$\dot{m}_a$ (kg/s)	7.1×10^{-5}	1.4×10^{-4}	1.1×10^{-4}	2.2×10^{-4}
$t_{w,in}$ (°C)	7.7×10^{-3}	1.0×10^{-2}	7.0×10^{-3}	1.1×10^{-2}

External walls of the domain are modeled as adiabatic. The mentioned simplification does not have a big impact on the correctness of the solution, because the difference between the temperature of external walls and ambient temperature is not so high. Heat transfer among working media is modeled as a coupled wall with an application of a shell conduction mechanism. Walls which separate both thermodynamic media are made from steel with a 5 mm thickness. Application of shell conduction mechanism allowed for heat conduction modeling in chamber walls not only in the normal direction but also along walls, which allows for obtaining a more accurate solution. Boundary conditions that occurred on deflector surfaces were defined also as adiabatic. The radiation emission factor for steel elements of the domain like walls and deflector is assumed as 0.7.

2.4. Physical Magnitudes Used for Heat Transfer Description

Numerical modeling results have been used for a description of the heat transfer phenomenon that occurred inside the combustion chamber. A heat flux density divided into a radiation and convection part has been used for it. Mentioned magnitudes have been used to describe of the overall amount of heat transferred to the cooling water by radiation and convection according to Equations (6) and (7).

$$\dot{Q}_{rad} = \iint_A \dot{q}_{rad} \cdot dA \tag{6}$$

$$\dot{Q}_{con} = \iint_A \dot{q}_{con} \cdot dA \tag{7}$$

The local value of the heat flux density has been used for calculation of the local distribution of a heat transfer coefficient. The heat transfer coefficient is known as a parameter describing the intensity of the occurred heat transfer process. The intensity of radiation and convection can be recognized separately based on radiation and convection heat transfer coefficient. The mentioned coefficients are calculated according to Equations (8) and (9).

$$\alpha_{rad} = \frac{\dot{q}_{rad}}{T_{bulk} - T_{wall}} \tag{8}$$

$$\alpha_{con} = \frac{\dot{q}_{con}}{T_{bulk} - T_{wall}} \tag{9}$$

The generic heat transfer coefficient is defined as a sum of the radiation and the convection factors. The heat transfer coefficient that occurred on the combustion chamber wall is dependent on a locally obtained difference between the wall temperature and the bulk-average temperature of exhaust gas. The bulk temperature of exhausts is achieved based on area-averaged temperature collected in subsequent horizontal cross-sections of the domain along to the Z dimension (Figure 3).

3. Results and Discussion

A comparison of exhaust gas temperature obtained during experimental and numerical research is shown in Figure 4. The temperature distribution is presented at four different heights of the combustion chamber representing properties obtained in three crucial parts of the chamber (two located in the burner neighborhood—bottom part, one halfway up, and one at the top of the chamber). It showed that the temperature of exhausts obtained during experimental measurements was lower relative to the numerical modeling. Especially it is well visible in the bottom part of the combustion chamber, where a temperature difference is much higher relative to higher parts of the chamber. The biggest divergence was obtained in the axis of the stand (above a burner). The highest noticed difference is equal to about 350 °C and was obtained for each of the analyzed cases. The temperature distinction decreases along the chamber radius in a wall direction. At a point located 5 cm away from the wall the temperature disparity for experimental and numerical analysis is lower and equals about 50 °C. A temperature distribution obtained during numerical modeling is getting closer to the experimental results as exhausts are moved away from the fixed bed in the vertical direction. Occurred temperature overestimation results from numerical modeling as an effect of the application of the Eddy Dissipation Model (EDM) of combustion [40,41]. EDM assumes that the realized combustion process is complete, which affects the temperature overestimation. Extermination of the mentioned phenomenon requires an application of the Eddy Dissipation Concept (EDC) model, which is an extension of EDM [42,43]. The EDC model is highly computationally expensive due to including a detailed chemical mechanism in a turbulent flow [44].
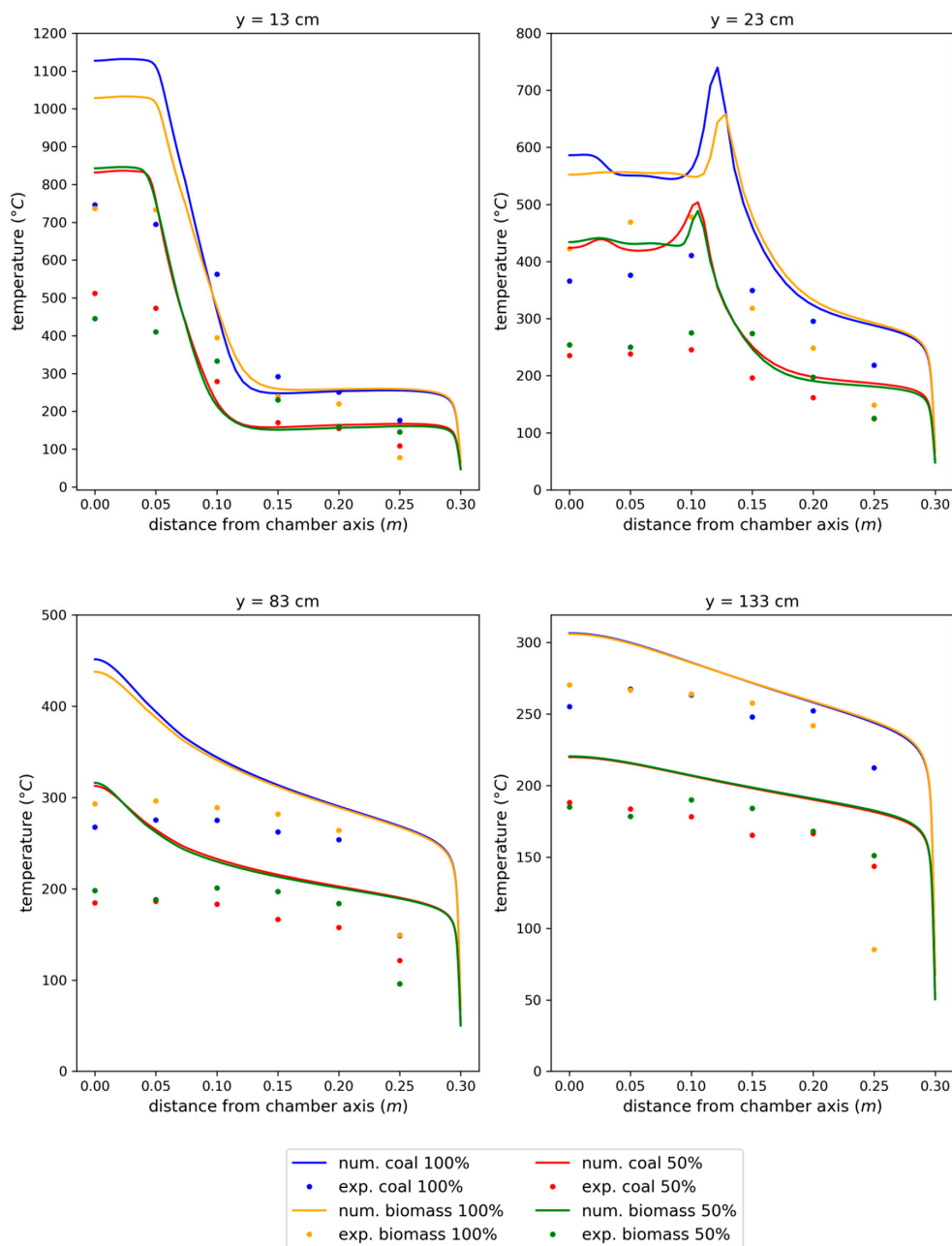
Figure 4. Comparison of an exhaust gas temperature distribution at different heights in the combustion chamber obtained from an experimental and a numerical part of the research.

Table 4 presents a comparison obtained for a few basic parameters connected with the combustion chamber working conditions during numerical modeling and experimental research for each of the analyzed cases. It is a heat flow transferred to the cooling water, the temperature of exhaust gas at the outlet from the domain, the temperature of cooling water at the outlet from the test stand, the cooling water temperature difference between outlet and inlet of the test stand, oxygen and carbon dioxide mass fraction in exhausts leaving the domain. Due to the inability of exhaust gas mass flow at the outlet from the combustion chamber during experimental research, the mentioned magnitude was compared with a result of analytical calculations. Time-averaged data collected during experimental research for each case separately comply with the results of numerical modeling. The amount of exhaust gas obtained during numerical simulations is consistent with analytical calculations. Collected parameters show convergence between numerical modeling and experimental validation.

Table 4. Comparison of crucial parameters obtained in numerical and experimental (analytical) part of the research.

Case	Experimental/Analytical Data				Numerical Data			
Fuel	Hard Coal		Biomass		Hard Coal		Biomass	
P_n (%)	50%	100%	50%	100%	50%	100%	50%	100%
$\dot{Q}$ (kW)	6.5	11.7	6.2	11.7	6.5	12.6	6.2	11.7
$t_{eg,out}$ (°C)	177.8	276.3	180.4	266.5	189.8	258.5	190.6	259.7
$\dot{m}_{eg,out}$ (kg/s)	0.80×10^{-2}	1.09×10^{-2}	0.75×10^{-2}	1.17×10^{-2}	0.80×10^{-2}	1.11×10^{-2}	0.75×10^{-2}	1.18×10^{-2}
$t_{w,out}$ (°C)	49.2	60.6	46.7	61.2	48.9	61.2	46.5	61.1
Δt_w (°C)	6.9	7.7	6.6	7.7	6.6	8.2	6.3	7.6
O_2, out (%)	14.2	10.0	13.8	11.2	13.9	9.6	14.1	11.6
CO_2, out (%)	7.0	10.1	7.0	9.1	7.4	10.8	9.8	12.5

Figure 5 shows a distribution of wall temperature and a bulk-average temperature inside the chamber as a function of the domain height. The temperature of the combustion chamber wall is generally constant. It only comes to a small rising of temperature in the direction of the working medium flow (from bottom to the top of the domain), which is related to the heating of water used for test stand cooling. The average bulk temperature of exhaust gas is noticeably changing in subsequent parts of the domain.
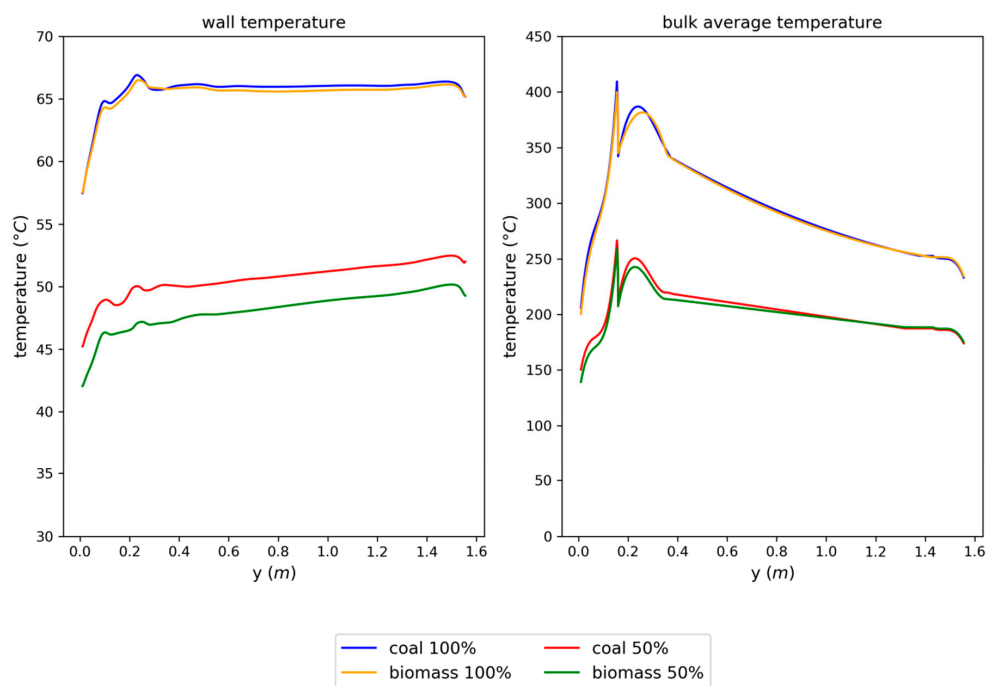
Figure 5. Distribution of exhaust gas temperature located in a layer neighboring with the combustion chamber wall and a bulk area-average temperature of flue gas as a function of chamber height.

The highest value is present in a direct neighborhood of a flame. It is following the obtained data concerning overall heat flux (sum of radiation and convection heat flux), which achieves maximum value in the mentioned area. The peak of the bulk temperature occurs in the area, where a deflector limits a flame length and smashes it horizontally. When fumes flow around a deflector, the average temperature deeply decreases. Right above a deflector comes the formation of an Eddy, which causes a significant cooling of flue gas (Figure 6). Over regions of swirled flow, a visible increase of bulk temperature is present. It is caused by exhausts getting through from the flame dispersion zone to the mentioned area. In the horizontal cross-sections of the chamber located above 20 cm over a deflector, the average temperature of exhausts is gradually decreasing. Exhausts flow in the upper part of a

chamber is more uniform than in the direct neighborhood of the deflector. When the gas has contact with the top surface of the combustion chamber it comes to obtain a backflow of a slight part of exhausts to the domain along heat transfer surface.
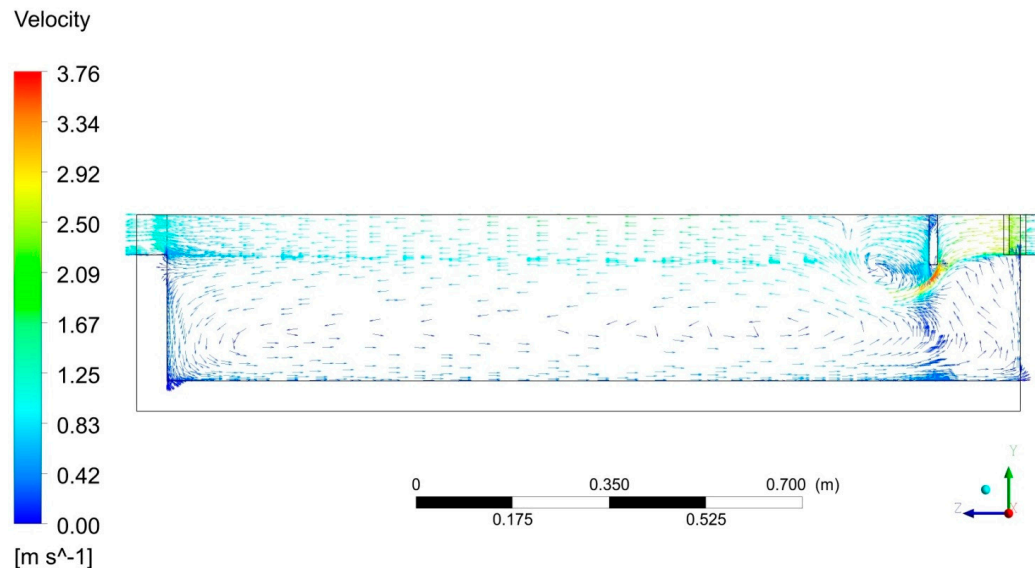

Figure 6. Visualization of the character of a flow inside a combustion chamber.

The local value of convection and radiation heat flux that occurred on the exhaust side of the combustion chamber wall along a domain height is present in Figure 7. Radiation and convection heat flux magnitudes are varied along with the height of the chamber. The impact of the radiation for an overall heat transfer process is dominating in the direct neighborhood of a flame. As a distance from a burning area is increased away, a local amount of the radiation heat flux is substantially falling off. The distribution of convective heat flux does not show significant changes over the entire surface bounding the combustion chamber. Regional increases depend on changes in the local value of the Reynolds Number and a thickness of a boundary layer. Determination of percentage participation in the heat transfer phenomenon for radiation and convection shows that they are dependent mainly on a heat load. During coal combustion with a nominal power, radiation is responsible for about 61.7% of the overall heat transfer. When combustion was carried out with the half level of the nominal heat load, radiation achieved only 50% in the heat transmission. Radiation participation in the heat transfer during biomass combustion was equal to 58.6% and 47.5%, respectively, for 100% and 50% of the nominal power.

Radiation and convection heat transfer coefficient courses are various for distinct parts of the computational domain (Figure 8). The radiation heat transfer coefficient achieves a peak in the direct neighborhood of a flame and vitally decreases in the upper part of the chamber, which is following in a radiation heat flux distribution. In the bottom part of the chamber, a radiation coefficient is uneven, which testifies with a differential level of the thermal load. A varied course of the convection heat transfer coefficient has occurred along with the domain height. In the direct neighborhood of the deflector, it comes to intense decreasing of α_{con}, which achieves a minimum value in the mentioned area. The convection heat transfer coefficient is increased in the area located above the deflector. After that, α_{con} is stabilized until a part of the domain, which is located 15 cm below the top surface of the domain. In the last part of the domain the top surface α_{con} achieves a maximum value. The peak value of the convection heat transfer coefficient is present also on the top surface of the combustion chamber. The main impact of the convection heat transfer is connected with the character of exhaust gas flow inside the combustion chamber (Figure 6). Exhaust gas movement occurred along a sidewall of the chamber and was an effect of reversing flow realized for a part of exhaust gas, which is not directly

conducted to the outlet. According to theory of heat transfer [45,46], Reynolds and Prandtl numbers are the main parameters used in the analytical description of the convection heat transfer coefficient. Figure 9 shows a distribution of Reynolds number obtained during the research for analyzed cases.
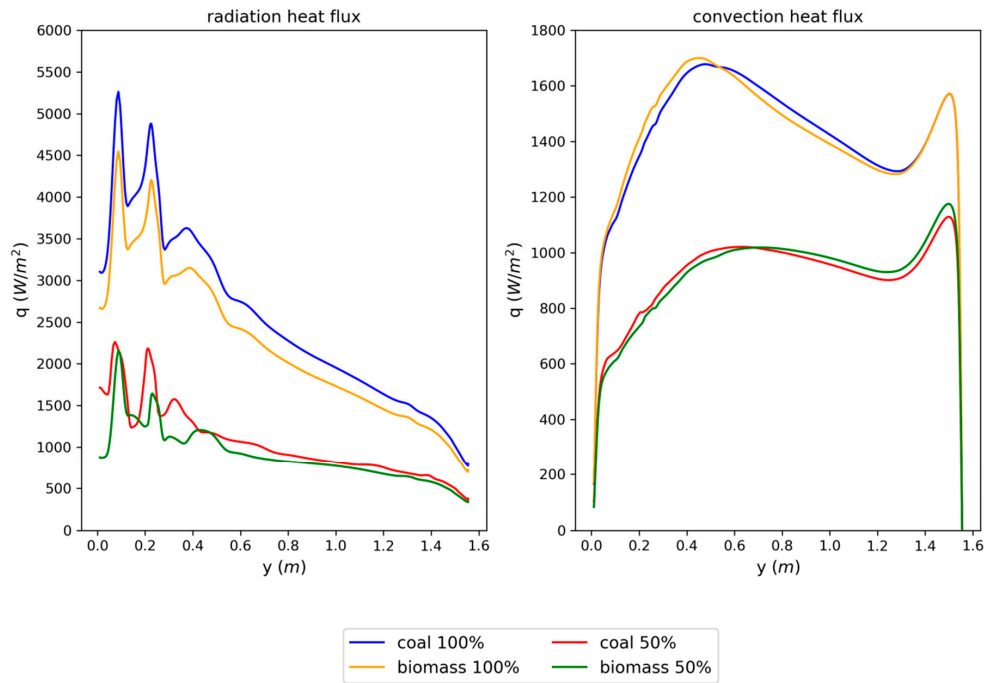

Figure 7. Distribution of radiation and convection heat flux obtained on the flue gas side of a chamber wall as a function of combustion chamber height.
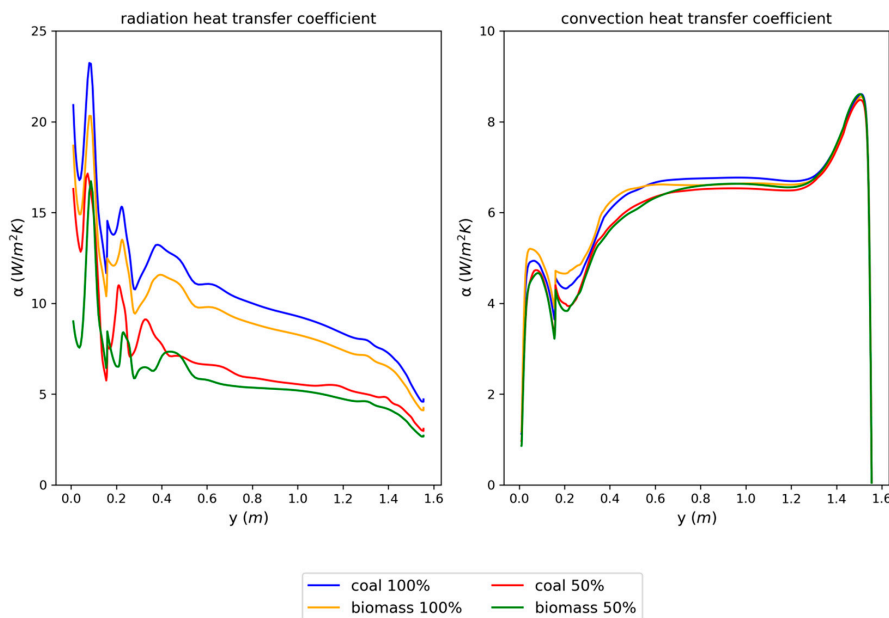

Figure 8. Distribution of radiation and convection heat transfer coefficient obtained on the flue gas side of a chamber wall as a function of combustion chamber height.
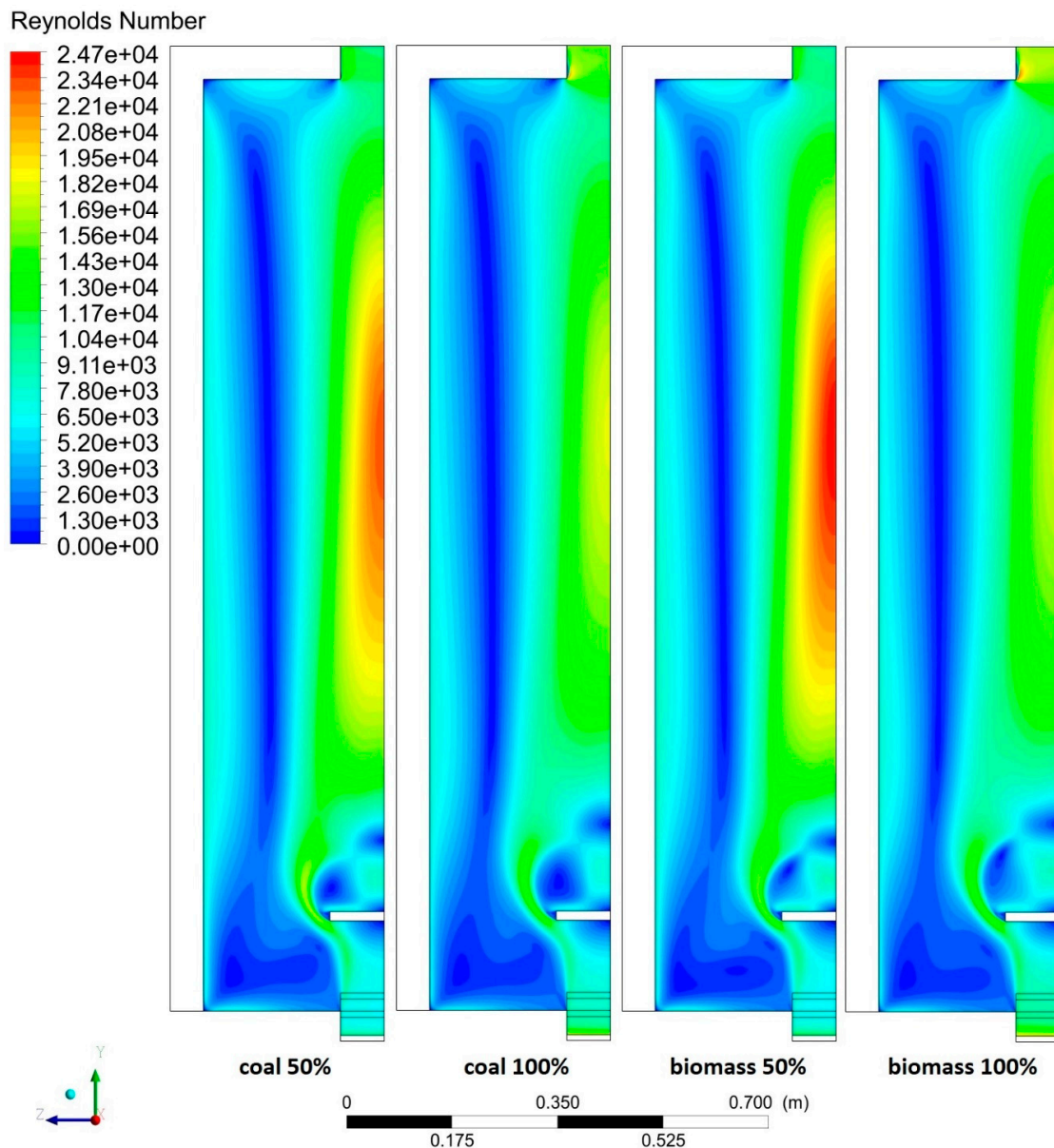
Figure 9. Reynolds number distribution obtained for each of the analyzed cases.

A diameter of the combustion chamber is used as a characteristic linear dimension in Reynolds number definition. In the direct neighborhood of the combustion chamber sidewall, Reynolds number achieves value corresponding to a laminar or transitional flow. The effect is visible in the obtained value of α_{con} which occurred during the mentioned types of fluid flow. A similar distribution of convection heat transfer coefficient between analyzed cases is connected with a lack of changes in Reynolds and Prandtl number distribution during fumes flow in the wall area.

4. Conclusions

The paper presented an experimental and numerical study on the combustion process of hard coal and biomass combustion in fixed bed conditions. Results of experimental validation and numerical modeling showed that:

- Numerical modeling of hard coal and biomass burning in fixed bed conditions allows simulating a heat transfer phenomenon that occurred in heating boilers to comply with experimental verification based on a fast chemistry model (Eddy dissipation). A numerical model to a certain

extent overestimates the temperature of exhaust gas. Elimination of the mentioned overestimation requires the application of a slow chemistry model (Eddy dissipation concept), which will be developed in further research on account of high computational expense. Percentage participation of radiation and convection during the heat transfer process mostly depends on the heat load of the heating device. As the test stand works with the lower heat load, a radiation impact is decreasing.

- Heat transferred by radiation was slightly lower during biomass combustion compared with coal burning. It has to do with a smaller temperature of combustion related to a lower heating value of biomass. A higher mass flow of exhaust present in the combustion chamber has an impact on a lower temperature of burning. A greater amount of exhaust results from the higher stream of biomass required for assurance of the same level of heating power. Likewise, biomass burning has to be realized with a higher excess air coefficient, which also has a big impact on a higher amount of exhaust gas present in the combustion chamber.

- Varied fuel properties and parameters of combustion do not have a visible impact on the convection heat transfer coefficient. The main influence for the mentioned factor is connected with a local temperature difference between the wall and exhaust gas located inside a combustion chamber.

- The distribution of Reynolds number obtained near to a sidewall of the combustion chamber does not show visible differences between analyzed cases. The main impact for a Reynolds number distribution in the central part of the combustion chamber is connected with the dynamic viscosity of a flue gas, which is a function of temperature. Higher mass flow of exhausts flowing through the combustion chamber during the nominal power caused a visible decrease of Reynolds number in the central area due to exhaust gas temperature rising despite an increase of flow velocity.

- The local value of radiation and convection heat transfer coefficient are effective parameters for recognition of intensity of the heat transfer process occurring inside a heating boiler combustion chamber during packed bed combustion. Thermal devices dealing with thermodynamic processes concerning fixed bed combustion have to deal with various thermal conditions occurring in different elements responsible for the heat transfer process. The application of fast chemistry modeling for simulating conditions that occur inside the combustion chambers of solid fuel boilers is a helpful tool in the design process. A complex shape combustion chamber used during packed bed combustion can be modernized with an appropriate calculation time bearing in mind a limitation imposed during the arrangement. The effect may be visible in higher thermal efficiency of the heating boiler because of better recognition of thermal conditions that occurred during various exploitation conditions. Moreover, the results of the modeling may be applied for the preparation of certain modifications in the analytical approach of a domestic and industrial boiler design process.

Conflicts of Interest: The author declares no conflict of interest.

Nomenclature

a	absorption coefficient	1/cm
A	area	m^2
b_1	Taylor-Foster approximation coefficient	m2/kg
b_T	Smith approximation coefficient	1/K
C_2	inertial loss coefficient	1/m
CO_2	mass fraction of carbon dioxide	%
D_p	diameter of the volume equivalent spherical particle	m
k	permeability	m^2
L	total height of the bed	m
LCV	low calorific value	MJ/kg
$\dot{m}$	mass flow	kg/s

O_2	mass fraction of oxygen	%
P_n	percentage level of heat load	%
t	temperature	°C
T	temperature	K
$\dot{q}$	heat flux density	W/m^2
$\dot{Q}$	heat flux, heating power	W
$\mathbf{v}_\propto$	superficial velocity	m/s
x	horizontal distance from a cylindrical chamber axis	m
y	vertical distance from a burner top surface	m
y^+	non-dimensional wall distance	dimensionless
α	heat transfer coefficient	Wm^{-2} K^{-1}
Δp	pressure drop	Pa
Δt	temperature difference	°C
ε	bed porosity	dimensionless
λ	excess air coefficient	dimensionless
μ	dynamic viscosity	Pa·s
ρ	density	kg/m^3

Abbreviations

a	air
ave	average
con	convection
eg	exhaust gas
exp	experimental
f	fuel
in	inlet
mea	measured
num	numerical
out	outlet
rad	radiation
s	soot
w	water

References

1. Statistics Poland. *Energy Consumption in Polish Households in 2018*; Statistics Poland: Warszawa, Poland, 2019. (In Polish)
2. Energy Regulatory Office. *Thermal Energy in Numbers—2019*; Energy Regulatory Office: Warszawa, Poland, 2020. (In Polish)
3. Statistics Poland. *Energy from Renewable Sources in 2018*; Statistics Poland: Warszawa, Poland, 2019.
4. Scharler, R.; Gruber, T.; Ehrenhöfer, A.; Kelz, J.; Bardar, R.M.; Bauer, T.; Hochenauer, C.; Anca-Couce, A. Transient CFD simulation of wood log combustion in stoves. *Renew. Energy* **2020**, *145*, 651–662. [CrossRef]
5. Wiese, J.; Wissing, F.; Höhner, D.; Wirtz, S.; Scherer, V.; Ley, U.; Behr, H.M. DEM/CFD modeling of the fuel conversion in a pellet stove. *Fuel Process. Technol.* **2016**, *152*, 223–239. [CrossRef]
6. Mehrabian, R.; Zahirovic, S.; Scharler, R.; Obernberger, I.; Kleditzsch, S.; Wirtz, S.; Scherer, V.; Lu, H.; Baxter, L.L. A CFD model for thermal conversion of thermally thick biomass particles. *Fuel Process. Technol.* **2012**, *95*, 96–108. [CrossRef]
7. Gómez, M.A.; Porteiro, J.; de la Cuesta, D.; Patiño, D.; Míguez, J.L. Numerical simulation of the combustion process of a pellet-drop-feed boiler. *Fuel* **2016**, *184*, 987–999. [CrossRef]
8. Gómez, M.A.; Porteiro, J.; De la Cuesta, D.; Patiño, D.; Míguez, J.L. Dynamic simulation of a biomass domestic boiler under thermally thick considerations. *Energy Convers. Manag.* **2017**, *140*, 260–272. [CrossRef]
9. Gómez, M.A.; Martín, R.; Chapela, S.; Porteiro, J. Steady CFD combustion modeling for biomass boilers: An application to the study of the exhaust gas recirculation performance. *Energy Convers. Manag.* **2019**, *179*, 91–103. [CrossRef]

10. Gómez, M.A.; Porteiro, J.; Patiño, D.; Míguez, J.L. Eulerian CFD modelling for biomass combustion. Transient simulation of an underfeed pellet boiler. *Energy Convers. Manag.* **2015**, *101*, 666–680. [CrossRef]

11. Mehrabian, R.; Shiehnejadhesar, A.; Scharler, R.; Obernberger, I. Multi-physics modelling of packed bed biomass combustion. *Fuel* **2014**, *122*, 164–178. [CrossRef]

12. Collazo, J.; Porteiro, J.; Patiño, D.; Granada, E. Numerical modeling of the combustion of densified wood under fixed-bed conditions. *Fuel* **2012**, *93*, 149–159. [CrossRef]

13. Ryfa, A.; Buczynski, R.; Chabinski, M.; Szlek, A.; Bialecki, R.A. Decoupled numerical simulation of a solid fuel fired retort boiler. *Appl. Therm. Eng.* **2014**, *73*, 794–804. [CrossRef]

14. Buczyński, R.; Weber, R.; Szlęk, A. Innovative design solutions for small-scale domestic boilers: Combustion improvements using a CFD-based mathematical model. *J. Energy Inst.* **2015**, *88*, 53–63. [CrossRef]

15. Chaney, J.; Liu, H.; Li, J. An overview of CFD modelling of small-scale fixed-bed biomass pellet boilers with preliminary results from a simplified approach. *Energy Convers. Manag.* **2012**, *63*, 149–156. [CrossRef]

16. Chapela, S.; Porteiro, J.; Míguez, J.L.; Behrendt, F. Eulerian CFD fouling model for fixed bed biomass combustion systems. *Fuel* **2020**, *278*, 118251. [CrossRef]

17. Tu, Y.; Yang, W.; Siah, K.B.; Prabakaran, S. Effect of different operating conditions on the performance of a 32 MW woodchip-fired grate boiler. *Energy Procedia* **2019**, *158*, 898–903. [CrossRef]

18. Tu, Y.; Zhou, A.; Xu, M.; Yang, W.; Siah, K.B.; Subbaiah, P. NOX reduction in a 40 t/h biomass fired grate boiler using internal flue gas recirculation technology. *Appl. Energy* **2018**, *220*, 962–973. [CrossRef]

19. Silva, J.; Teixeira, J.; Teixeira, S.; Preziati, S.; Cassiano, J. CFD Modeling of Combustion in Biomass Furnace. *Energy Procedia* **2017**, *120*, 665–672. [CrossRef]

20. Rezeau, A.; Díez, L.I.; Royo, J.; Díaz-Ramírez, M. Efficient diagnosis of grate-fired biomass boilers by a simplified CFD-based approach. *Fuel Process. Technol.* **2018**, *171*, 318–329. [CrossRef]

21. Bermúdez, C.A.; Porteiro, J.; Varela, L.G.; Chapela, S.; Patiño, D. Three-dimensional CFD simulation of a large-scale grate-fired biomass furnace. *Fuel Process. Technol.* **2020**, *198*, 106219. [CrossRef]

22. Klason, T.; Bai, X.S.; Bahador, M.; Nilsson, T.K.; Sundén, B. Investigation of radiative heat transfer in fixed bed biomass furnaces. *Fuel* **2008**, *87*, 2141–2153. [CrossRef]

23. Joachimiak, M.; Joachimiak, D.; Ciałkowski, M.; Małdziński, L.; Okoniewicz, P.; Ostrowska, K. Analysis of the heat transfer for processes of the cylinder heating in the heat-treating furnace on the basis of solving the inverse problem. *Int. J. Therm. Sci.* **2019**, *145*, 105985. [CrossRef]

24. Rezazadeh, N.; Hosseinzadeh, H.; Wu, B. Effect of burners configuration on performance of heat treatment furnaces. *Int. J. Heat Mass Transf.* **2019**, *136*, 799–807. [CrossRef]

25. Yıldız, E.; Başol, A.M.; Mengüç, M.P. Segregated modeling of continuous heat treatment furnaces. *J. Quant. Spectrosc. Radiat. Transf.* **2020**, *249*, 106993. [CrossRef]

26. Gautam, A.; Saini, R.P. Experimental investigation of heat transfer and fluid flow behavior of packed bed solar thermal energy storage system having spheres as packing element with pores. *Sol. Energy* **2020**, *204*, 530–541. [CrossRef]

27. Barde, A.; Nithyanandam, K.; Shinn, M.; Wirz, R.E. Sulfur heat transfer behavior for uniform and non-uniform thermal charging of horizontally-oriented isochoric thermal energy storage systems. *Int. J. Heat Mass Transf.* **2020**, *153*, 119556. [CrossRef]

28. Ziegler, B.; Mosiężny, J.; Czyżewski, P. Unsteady CHT analysis of a solid state, sensible heat storage for PHES system. *Int. J. Numer. Methods Heat Fluid Flow* **2019**. [CrossRef]

29. Taler, D.; Taler, J.; Trojan, M. Thermal calculations of plate–fin–and-tube heat exchangers with different heat transfer coefficients on each tube row. *Energy* **2020**, *203*, 117806. [CrossRef]

30. Li, N.; Chen, J.; Cheng, T.; Klemeš, J.J.; Varbanov, P.S.; Wang, Q.; Yang, W.; Liu, X.; Zeng, M. Analysing thermal-hydraulic performance and energy efficiency of shell-and-tube heat exchangers with longitudinal flow based on experiment and numerical simulation. *Energy* **2020**, *202*, 117757. [CrossRef]

31. Judt, W.; Bartoszewicz, J. Analysis of fluid flow and heat transfer phenomenon in a modular heat exchanger. *Heat Transf. Eng.* **2019**, in press. [CrossRef]

32. ANSYS Inc. *ANSYS FLUENT User Guide*; 18.2.; ANSYS Inc.: Canonsburg, PA, USA, 2017.

33. Vasquez, E.R.; Eldredge, T. Process modeling for hydrocarbon fuel conversion. In *Advances in Clean Hydrocarbon Fuel Processing: Science and Technology*; Elsevier Ltd.: Amsterdam, The Netherlands, 2011; pp. 509–545. ISBN 9781845697273.

34. ANSYS Inc. *ANSYS Fluent Theory Guide*; 18.2; ANSYS Inc.: Canonsburg, PA, USA, 2017.

35. Tae-Ho, S. Comparison of engineering models of nongray behavior of combustion products. *Int. J. Heat Mass Transf.* **1993**, *36*, 3975–3982. [CrossRef]

36. Sazhin, S.S. *An Approximation for the Absorption Coefficient of Soot in a Radiating Gas*; Manuscript, Fluent Europe, Ltd.: Sheffield, UK, 1994.

37. Smith, T.F.; Shen, Z.F.; Friedman, J.N. Evaluation of coefficients for the weighted sum of gray gases model. *J. Heat Transf.* **1982**, *104*, 602–608. [CrossRef]

38. Taylor, P.B.; Foster, P.J. The total emissivities of luminous and non-luminous flames. *Int. J. Heat Mass Transf.* **1974**, *17*, 1591–1605. [CrossRef]

39. TNO Phyllis 2. Available online: https://phyllis.nl/ (accessed on 8 September 2020).

40. Zubanov, V.M.; Stepanov, D.V.; Shabliy, L.S. The technique for Simulation of Transient Combustion Processes in the Rocket Engine Operating with Gaseous Fuel "hydrogen and Oxygen". *J. Phys. Conf. Ser.* **2017**, *803*, 012187. [CrossRef]

41. Yadav, S.; Mondal, S.S. Modelling of oxy-pulverized coal combustion to access the influence of steam addition on combustion characteristics. *Fuel* **2020**, *271*, 117611. [CrossRef]

42. Jójka, J.; Ślefarski, R. Dimensionally reduced modeling of nitric oxide formation for premixed methane-air flames with ammonia content. *Fuel* **2018**, *217*, 98–105. [CrossRef]

43. Lewandowski, M.T.; Parente, A.; Pozorski, J. Generalised Eddy Dissipation Concept for MILD combustion regime at low local Reynolds and Damköhler numbers. Part 1: Model framework development. *Fuel* **2020**, *278*. [CrossRef]

44. Bösenhofer, M.; Wartha, E.M.; Jordan, C.; Harasek, M. The eddy dissipation concept-analysis of different fine structure treatments for classical combustion. *Energies* **2018**, *11*, 1902. [CrossRef]

45. Rohsenow, W.; Hartnett, J. *Handbook of Heat Transfer*; McGraw-Hill Education: New York, NY, USA, 1999; ISBN 0070535558.

46. Serth, R.W. *Process Heat Transfer: Principles and Applications*; Elsevier Academic Press: Cambridge MA, USA, 2007; ISBN 9780080544410.

Publisher's Note: MDPI stays neutral with regard to jurisdictional claims in published maps and institutional affiliations.

Errata do artykułu

Judt W., Numerical and Experimental Analysis of Heat Transfer for Solid Fuels Combustion in Fixed Bed Conditions, Energies, vol. 13, is. 22, pp. 6141: 1-18, 2020.

W opublikowanym artykule dane w tabeli 3 na stronie 8 doszło do przesunięcia danych na skutek błędu redakcyjnego. W związku z powyższym poniżej zamieszczono poprawnie zredagowaną tabelę.

Table 3. Crucial physical magnitudes used as boundary conditions in the inlet to the numerical domain.

fuel	hard coal		biomass	
P_n (%)	**50%**	**100%**	**50%**	**100%**
$\dot{m}_w$ [kg/s]	$5.7 \cdot 10^{-2}$	$9.2 \cdot 10^{-2}$	$5.7 \cdot 10^{-2}$	$9.2 \cdot 10^{-2}$
$\dot{m}_f$ [kg/s]	$7.1 \cdot 10^{-5}$	$1.4 \cdot 10^{-4}$	$1.1 \cdot 10^{-4}$	$2.3 \cdot 10^{-4}$
$\dot{m}_a$ [kg/s]	$1.9 \cdot 10^{-3}$	$2.6 \cdot 10^{-3}$	$1.7 \cdot 10^{-3}$	$2.7 \cdot 10^{-3}$
$t_{w,in}$ [°C]	42.3	53.0	40.2	53.5